7-30-2019

# Density Matrix Renormalization Group Studies of Interacting Dipoles in a Zigzag Chain

Niraj Ghimire
*University of Connecticut - Storrs*, niraj.ghimire@uconn.edu

# Density Matrix Renormalization Group Studies of Interacting Dipoles in a Zigzag Chain

Niraj R. Ghimire, Ph.D.
University of Connecticut, 2019

## ABSTRACT

In this dissertation, we study the many-body effects of dipoles in a quasi-one-dimensional zigzag optical lattice, which we call the zigzag chain. We study this system using the Density Matrix Renormalization Group (DMRG) method, which has established itself as the most powerful numerical method to simulate one-dimensional lattices. For the implementation of DMRG, we have used the open-source package Intelligent Tensor, or simply ITensor. The first part of this research focuses on dipoles polarized in the plane of the zigzag chain by an external electric field with the condition that the dipoles can hop around and interact with their first and second neighbors and the number of dipoles is exactly a half of the number of lattice sites. With the interactions much stronger than the hopping, the system comprises of frustrated and non-frustrated regimes owing to the combination of attractive and repulsive

interactions in different directions. The consequence is a complex phase diagram featuring the trivial ferromagnetic and antiferromagnetic phases as well as the non-trivial dimerized and superfluid phases. The second part of the research deals with randomly oriented dipoles in the zigzag chain such that each lattice site has exactly one dipole and each dipole interacts with its first and second neighbors but in the absence of any hopping. We study the second system classically allowing many different orientations for each dipole in a lattice site as well as quantum mechanically by allowing a few quantized degrees of freedom to each dipole. The result is a phase diagram showing ferromagnetic, antiferromagnetic and paramagnetic phases.

# Density Matrix Renormalization Group Studies of Interacting Dipoles in a Zigzag Chain

Niraj R. Ghimire

M.S. Physics, University of Connecticut, Storrs, CT, 2013

A Dissertation
Submitted in Partial Fulfillment of the
Requirements for the Degree of
Doctor of Philosophy
at the
University of Connecticut

2019

**APPROVAL PAGE**

Doctor of Philosophy Dissertation

# Density Matrix Renormalization Group Studies of Interacting Dipoles in a Zigzag Chain

Presented by
Niraj R. Ghimire, M.S.

Major Advisor _____
Susanne Yelin

Associate Advisor _____
Juha Javanainen

Associate Advisor _____
Robin Cote

University of Connecticut
2019

*For Sushma, my beloved wife*

# ACKNOWLEDGEMENTS

I would like to thank everyone who made this dissertation possible by helping me through this long and arduous journey of my doctorate degree. My deepest gratitude goes to my advisor Dr. Susanne Yelin for her immense support and guidance throughout my graduate career. The level of motivation and encouragement that I have received from her is outstanding, and I feel proud to have her as my mentor. I also thank my associate advisors Dr. Juha Javanainen and Dr. Robin Cote for their help and support. Additionally, I would also like to express my gratitude to all the faculty in the physics department who helped me in one way or the other, especially Dr. Jason Hancock, Dr. Diego Valente, Dr. Boris Sinkovic, Dr. Gerald Dunne, Dr. Michael Rozman, Dr. Richard Jones, Dr. Thomas Blum, Dr. Douglas Hamilton, Dr. Barrett Wells, Dr. Gayanath Fernando, Dr. Ilya Sochnikov, Dr. Alexander Balatsky, Dr. Menka Jain and Dr. Daniel McCarron. I would also like to thank former physics department staff Kim, Dawn, Barbara, Heather and Ann Marie as well as the current staff Alessandra, Micki, Carrie, Anna and Sarah for all of their help. I am highly appreciative of all the help I received from my group members Belter, Efi, Florentin, Phillip, Hanzhen and Robert. My special thanks goes to my group member Qing with whom I have had many insightful discussions. I also thank Dr. Hannes Pichler (Harvard University) for helpful discussions. I am extremely grateful to Dr. Edwin Miles Stoudenmire, the lead developer of the C++ library Intelligent Tensor (ITensor), for helping me write the codes for my research projects and checking them for errors.

My sincere thanks goes to Dr. Robin Grenier (Neag School of Education), Dr. Aynsley Diamond (Center of Excellence in Teaching and Learning) and Dr. Dan Eustace (Department of Chemistry) who have had a great impact on my professional development.

Additionally, I am grateful to my friends in the physics department for their valuable time and support - Sahan, Sanka, James, Ionel, Asanka, Amani, Kemal, Matthew, Erin and Gabe - just to name a few, and to my friends in the Nepalese community in Storrs, especially Ramesh KC (Office of the Bursar) and Dr. Hari P. Koirala (Eastern Connecticut State University).

Finally, I would like to thank my late father who worked hard all of his life to raise me, my mother and sister for their love, my wife Sushma for being by my side in the toughest times of my life, and my son Yuvan who inspires me everyday to find smarter ways to deal with challenges.

# TABLE OF CONTENTS

# LIST OF FIGURES

# Chapter 1

# Introduction

## 1.1 Ultracold atoms and molecules in optical lattices

Ultracold atoms and molecules serve as an ideal platform to study quantum-many body systems in a various fields ranging from condensed-matter physics to high-energy physics [1, 2]. Ultracold experiments are performed using an optical lattice, which is an artificial periodic array produced by interfering several laser light beams and which resembles the periodic lattice of real solid-state crystals. Atoms, ions and molecules can be trapped in such an array by adjusting the electric field of the interfering laser beams [3]. What is so special about the optical lattices? Not only can the geometry, dimensionality, disorder and depth of the lattice be controlled to a high degree, lattices can be produced to carry artificial magnetic fields [4] several orders of magnitude larger than the strongest magnetic fields created in solid-state laboratories, thus allowing to investigate topological quantum matter with ultracold atoms [1].

With ultracold atoms, quantum systems can be engineered to be isolated from the environment, thus allowing the exploration of fundamental phenomena in statistical physics. How does a closed, isolated quantum system obtain

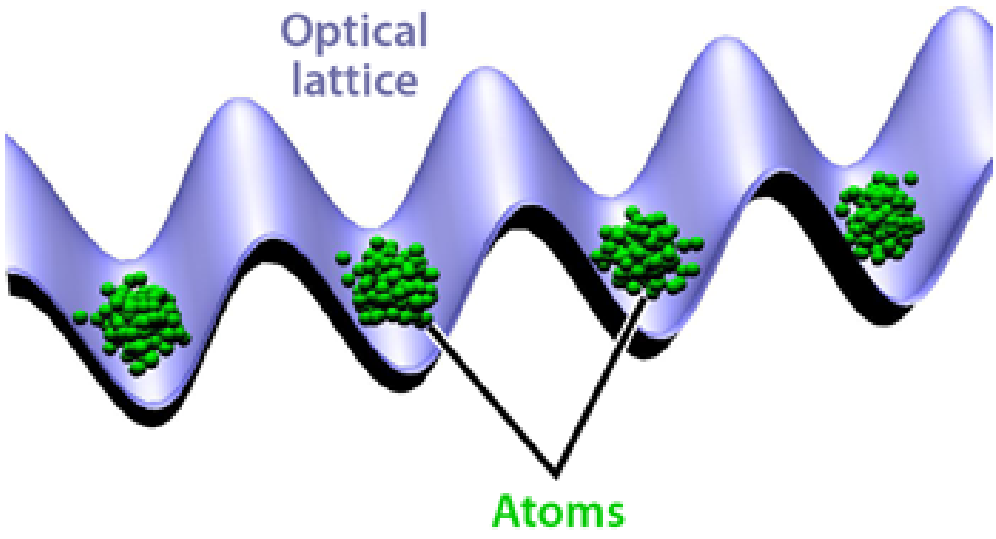


Figure 1.1.1: (Color online) An optical lattice with several atoms in each site. Taken from [5].

a temperature and thermalize during its quantum evolution [6, 7, 8]? What type of closed quantum system fails to thermalize even after a long quantum evolution? Experiments with ultracold atoms and ions are at the core of these fundamental research questions [9, 10] that challenge the foundations of statistical physics and thermodynamics.

Ultracold bosonic and fermionic quantum gases provide a solid platform to probe fundamental problems in condensed-matter physics [11, 12, 13, 14, 15, 16, 17, 18, 19, 20, 21, 22, 23] and to find applications in quantum optics and quantum information processing [24]. By storing such ultracold quantum gases in artificial periodic potentials of light, it has been possible to create structures way beyond those currently achievable in condensed-matter physics systems [11].

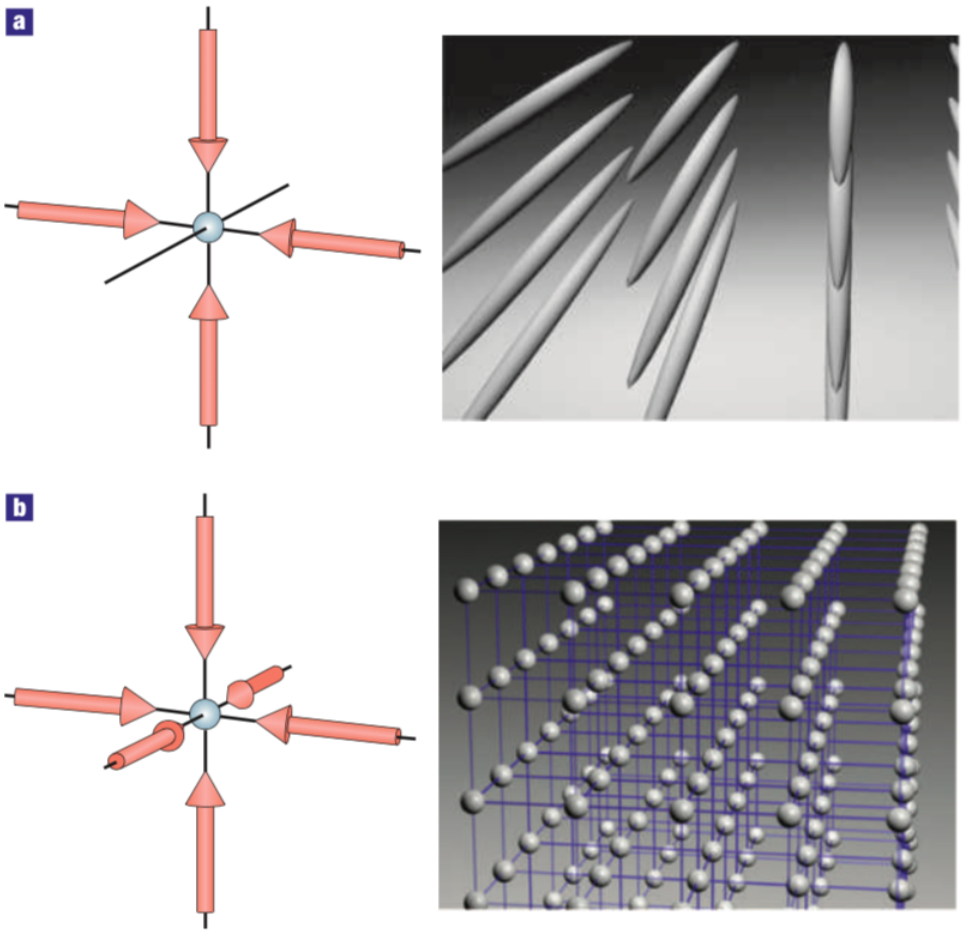


Figure 1.1.2: (Color online) (a) Two-dimensional optical lattice produced by interfering two orthogonal standing waves where the atoms are trapped in the one-dimensional potential tubes. (b) Three-dimensional optical lattice obtained by superposing three orthogonal standing waves. The lattice resembles a simple cubic array and each site is associated with a harmonic oscillator potential in which atoms are confined. Taken from [11].

The first strongly correlated lattice model to have been realized with ultracold atoms is the Bose-Hubbard model [14], and this is still a prominent model in ultracold experiments. The simple but intriguing model contains three parameters: The nearest-neighbor tunneling strength $t$ describes the motion of the atoms in the lattice, the mutual interaction of the atoms on the same lattice site is described by the on-site potential $U$, and the spatial confinement

due to the laser beams produces a site-dependent energy shift $V_i$ where $i$ is the site index. By decreasing the ratio $t/U$, the system can be driven from the superfluid to the strongly correlated Mott-insulating phase.

The realization of Fermi-Hubbard model is another active problem in ultracold experiments [25]. The motivation behind this problem is the strong connection to high-temperature superconductors [26, 27, 28], where the Hubbard model is often used to model the effective electronic degrees of freedom. The interaction between ultracold lattice fermions is controlled by the external magnetic field via Feshbach resonances [29] while the doping is determined by the atom number, setting the chemical potential in the system. As the ratio of $U/t$ is increased, finite-temperature, half-filled repulsively interacting Fermi-Hubbard systems undergo a crossover from the metallic to Mott-insulating phase, where half-filled means that the system is in the undoped regime of one atom per lattice site and has equal numbers of both spin components.

Although atoms interact via short-range contact interactions in most cold atom experiments, many-body systems with longer-range interactions are predicted to exhibit intriguing quantum phases [1, 30, 31, 32]. Currently under study are three different approaches to induce long-range interactions via ultracold atoms: The first approach is by using strongly magnetic atomic species such as chromium [33], dysprosium [34] and erbium [35], the second is based on ground state polar molecules [36, 37, 38], and the third is by using the extremely strong van der Waals interactions between Rydberg states [39].

## 1.2 Quantum simulation

Simulating quantum mechanics is a very challenging problem, as was realized in the early 1980s [40, 41]. The major problem is the amount of computer memory needed to store the quantum state of a large physical system. The number of parameters required to describe this state grows exponentially with the system size. However, this problem may be solved by using some controllable quantum system to study another less controllable quantum system, the approach known as quantum simulation [2]. A quantum simulator should not be confused with the "quantum computer" as proposed by Richard Feynman in 1982 [41]. As has become clear over the past three decades, a quantum computer may possess capabilities way beyond quantum simulation, and therefore, quantum computation and quantum information theory have become very active research fields in the recent years [42, 43, 44]. The quantum machine proposed by Feynman would have the capacity to store an exponentially large amount of information without using an exponentially large amount of physical resources, thus making it an ideal tool for quantum simulation. It was shown a decade later that a quantum computer can act an an universal quantum simulator, where the word universal means except for changes in the programs that it runs, the same machine is capable of solving many different problems [2]. However, a universal quantum computer is not needed for implementing quantum simulation. Simpler quantum devices that reproduce the

physics of more sophisticated quantum systems could be used for this purpose (these are problem-specific machines rather than universal simulators). Therefore, practical quantum simulation is expected to be a reality much sooner than full-fledged quantum computers.

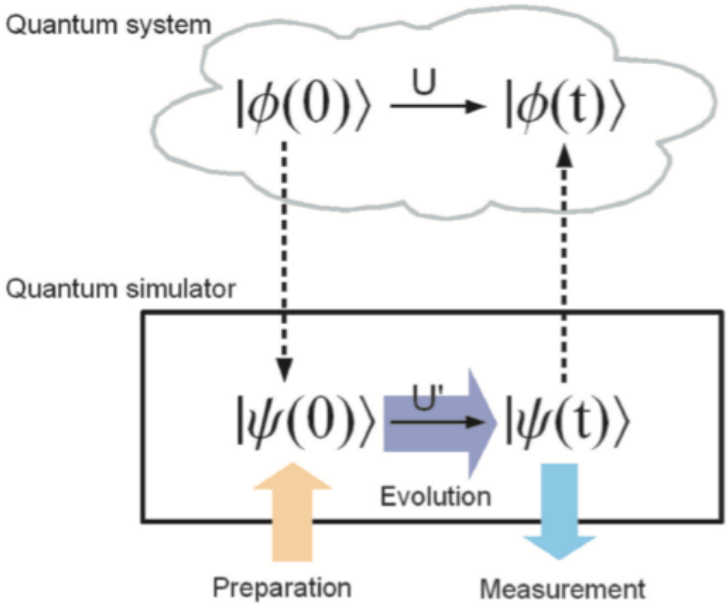


Figure 1.2.1: (Color online) The quantum state $|\phi(0)\rangle$ of a real quantum system evolves in time to the state $|\phi(0)\rangle$ via the unitary transformation $U = \exp(-i\hbar H_{\text{sys}}t)$. At the same time, the quantum simulator that mimics this quantum system evolves from the state $|\psi(0)\rangle$ to the state $|\phi(t)\rangle$ via the unitary transformation $U' = \exp(-i\hbar H_{\text{sim}}t)$. There exists a mapping between the system and the simulator: $|\phi(0)\rangle \leftrightarrow |\psi(0)\rangle, |\phi(t)\rangle \leftrightarrow |\psi(t)\rangle$ and $U \leftrightarrow U'$. Taken from [2].

In recent years, the interest in quantum simulation has soared for two reasons. First, it has potential application in a variety of fields ranging from condensed-matter physics to chemistry and even biology. For instance, in condensed-matter physics, quantum simulation would take us closer to understanding interesting phenomena such as quantum phase transitions, quantum mag-

netism and high-temperature superconductivity [2]. Second, the technologies required for the coherent control of quantum systems have evolved so much that the physical implementation of quantum simulation looks accessible very soon, considering the fact that some proof-of-principle experiments have already been realized [14, 45, 46, 47, 48, 49, 50].

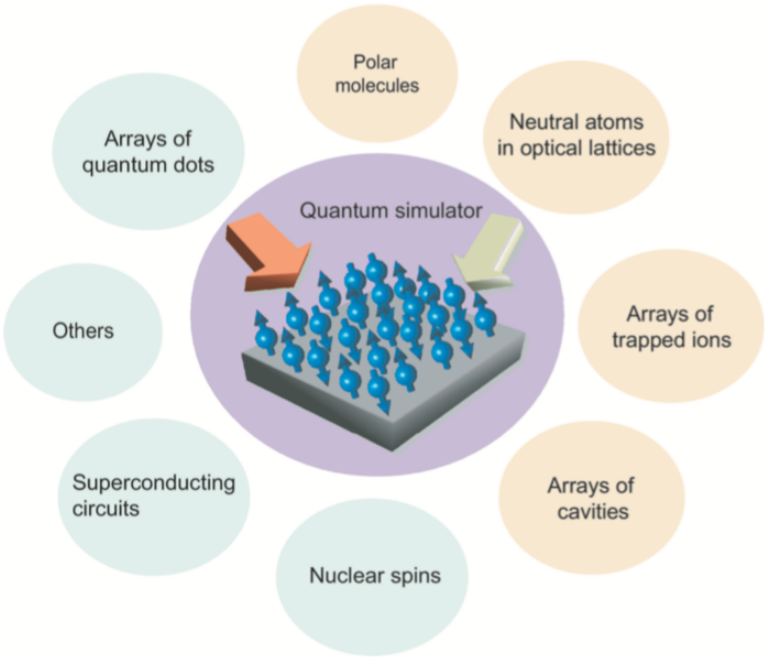


Figure 1.2.2: (Color online) Various systems that could be used as quantum simulators to study the problems in condensed-matter physics. Taken from [2].

Because the geometry, dimension, disorder and depth of an optical lattice can be controlled to a high degree, ultracold atom-based simulators have already been used to investigate quantum many-body problems, especially those so complex that they cannot be solved even on today's most powerful classical supercomputers [1]. There has been increasing interest in the study of condensed-matter physics with atoms in optical lattices since the first experi-

ment on the simulation of the quantum phase transition from a superfluid to a Mott insulator using a cold atomic gas in an optical lattice [14]. Atoms in optical lattices have several controllable parameters such as tunneling strength, on-site, nearest-neighbor, and long-range interaction, non-uniform potentials, etc. In addition, both bosonic and fermionic elements can be used for quantum simulation with atoms in optical lattices [2].

## 1.3 Frustrated quantum systems

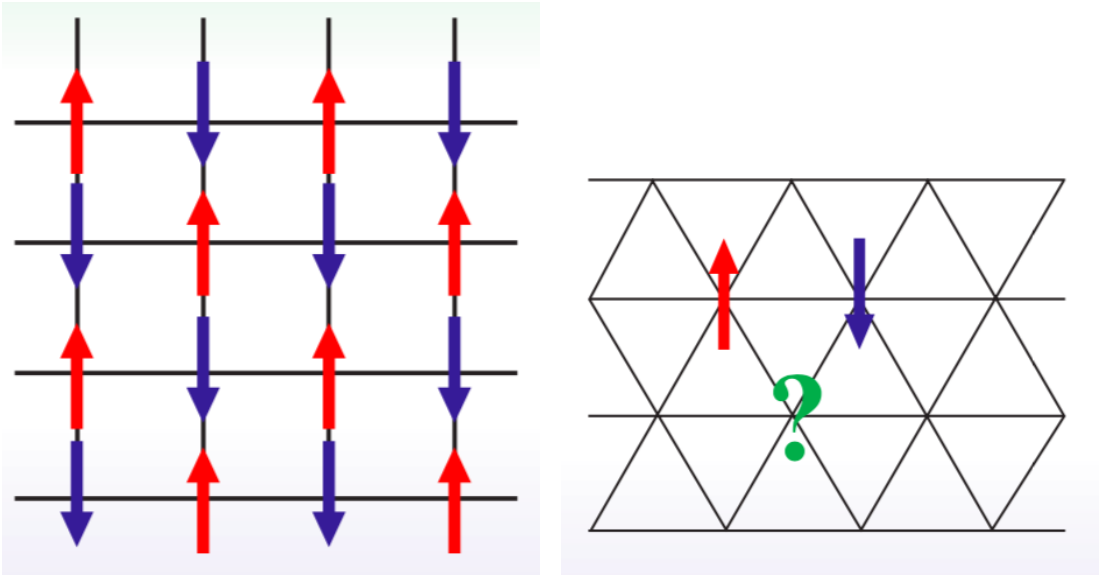


(a) Non-frustrated spins on a square lattice (b) Frustrated spins on a triangular lattice

Figure 1.3.1: (Color online) (a) Each spin on a square lattice can be pairwise antialigned with all its neighbors resulting in an antiferromagnet. (b) Three spins on a triangular lattice cannot be pairwise antialigned and therefore, the system is frustrated. Taken from [51].

A tremendous amount of work has been done in equilibrium statistical mechanics to understand the basic mechanisms responsible for spontaneous ordering as well as the nature of the phase transition in many physical systems [53]. In

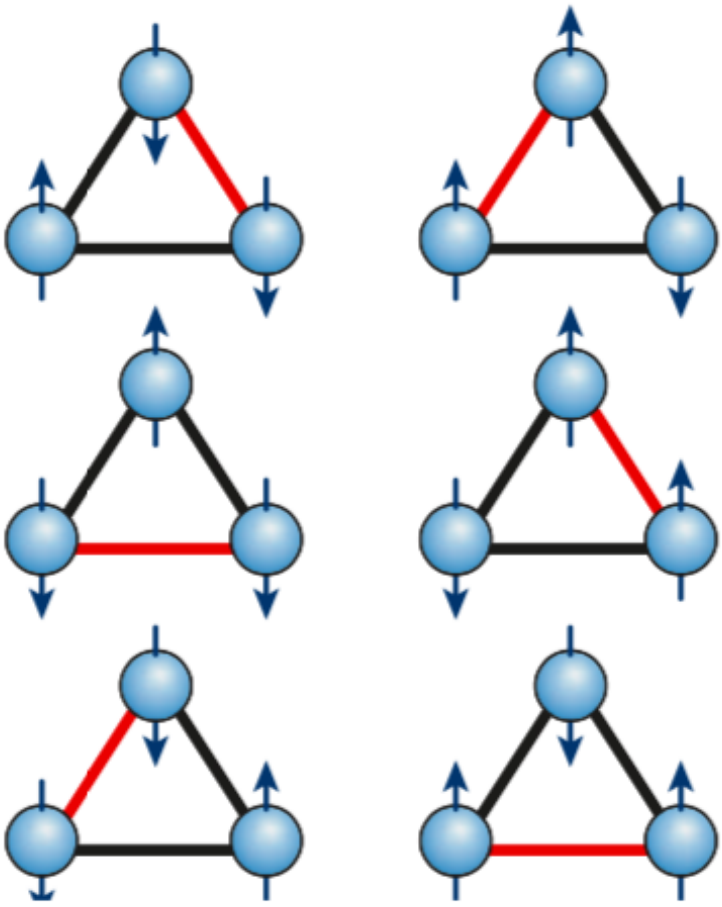

Figure 1.3.2: (Color online) If the interaction between the spins at the corners of a triangle is antiferromagnetic, then the spins cannot be pairwise antialigned. Therefore, the ground state is six-fold degenerate, i.e., all the six configurations shown here have the same energy. Taken from [52].

this context, frustrated models have received much attention over the past few decades [54]. The word "frustration" has been introduced [55, 56] to refer to the situation where a spin (or a number of spins) in a lattice cannot find an alignment to fully satisfy the interactions with its neighbors as shown in Figure 1.3.1b and Figure 1.3.2. Real magnetic materials such as disordered systems, systems with long-range interaction, and three-dimensional systems, to name

a few, are often frustrated due to several kinds of interactions. The effects of frustrations are often unexpected, and many of them are not understood yet. Recent studies show that many established statistical methods and theories have struggled to explain the phenomena observed in frustrated systems. Therefore, frustrated systems are often considered excellent candidates to improve theories and find better approximations [53]. Additionally, the concept of frustration has a very important role on spin systems, including Ising spin systems, classical vector spin systems such as XY model, classical Heisenberg model, and so on, as well as quantum spin systems. The spin glasses are one of the most interesting problems in the spin systems in which the frustration plays an important role.

The search for spin liquid behavior has been one of the main challenges of quantum magnetism ever since the proposal was made by Anderson [57, 58]. Spin liquid phases, which are phases with no long-range Neel order, are expected to be stabilized in low dimensions or in the presence of frustration, a situation where quantum fluctuations can strongly suppress magnetism. It gives rise to exotic low-energy excitations whose properties can only be investigated fully using non-perturbative techniques. In the two-dimensional case, different spin liquid phases have been found and feature bond ordering or topological ordering [53, 59, 60]. In one dimension, the Mermin-Wagner theorem [61] suggests that quantum fluctuations give rise to disordered ground state in systems with a continuous symmetry, which means a spin liquid phase is expected.

The one-dimensional case is preferred because several non-perturbative techniques are available to fully characterize the physical properties of different spin liquids. These powerful techniques include intergrability, conformal field theory (CFT) [62, 63], the bosonization approach [64, 65, 66] and the density matrix renormalization group (DMRG) approach [67, 68].

## 1.4 Density Matrix Renormalization Group (DMRG)

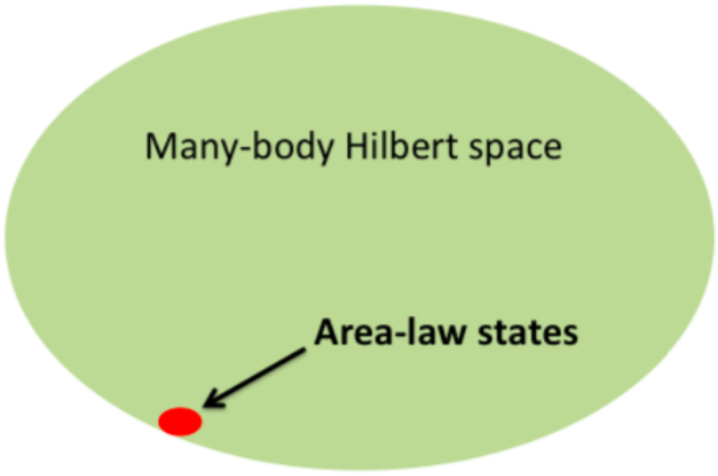


Figure 1.4.1: (Color online) The quantum states that obey the area- law for the entanglement entropy correspond to a tiny corner of the full Hilbert space. Taken from [69].

The Hilbert space of a many-body system is too large for a classical computer to deal with. For a system of $N$ spin-1/2 particles, for example, the dimension of the Hilbert space is $2^N$, and therefore, the search for the ground state in such a large space of configurations is a daunting task. It can be proven that the low-energy eigenstates of gapped Hamiltonians (i.e., the Hamiltonians that have a

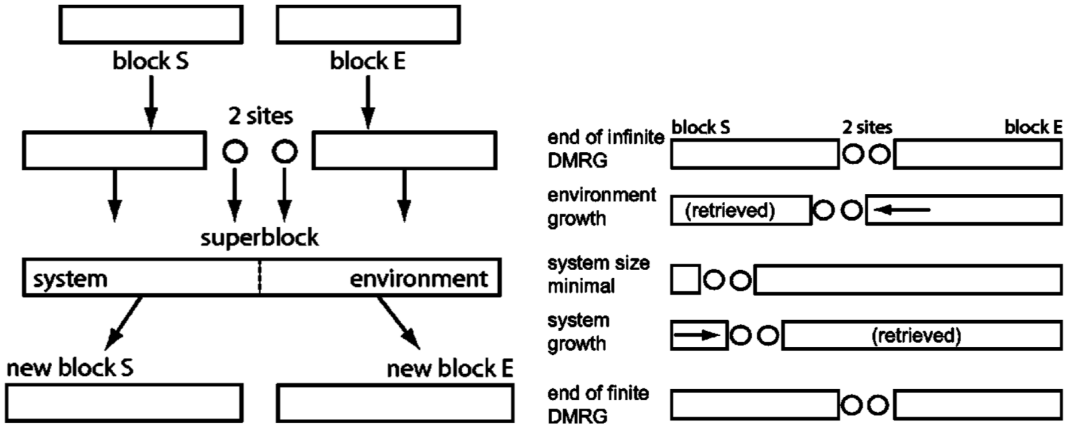


(a) Infinite-system DMRG (b) Finite-system DMRG

Figure 1.4.2: Taken from [70].

gap between the ground state and the first excited state) with local interactions (i.e., the interactions only between nearest and next-nearest neighbors) obey the so-called area-law for the entanglement entropy, and these eigenstates lie in a very small subspace of the Hilbert space as shown in Figure 1.4.1. The remarkable feature of this subspace is that it can be parametrized efficiently with limited numerical resources and efficient algorithms such as the DMRG to address important questions of quantum physics. The parameterization is done using matrix product states. We acknowledge that besides DMRG, there are other numerical methods to simulate one dimensional systems such as Time-Evolving Block Decimation (TEBD) and Power Wave Function Renormalization Group (PWFRG) but their discussion is outside of the scope of this thesis.

DMRG is a numerical variational technique formulated by Steven R. White in 1992 [67] to study the low energy physics of quantum many-body systems. It is regarded as the most efficient numerical method for one-dimensional systems.

The key idea of DMRG is to study the many-body properties of a system by increasing its size gradually, truncating the Hilbert space repeatedly and keeping only the most important states of the system and tracing out the unimportant ones. The lattice is divided into two blocks, one is treated as the "system", $S$, while the other is treated as the "environment", $E$. Assuming that we are looking for the ground state, the algorithm for infinite-system DMRG is formulated as follows [70]:

(1) Suppose the system block $S$ is of size $l$ and we know the Hamiltonian and the ground state. Suppose $M^S$ be the size of the Hilbert space in which S lives. Similarly, construct an environment block $E$ of size $l$.

(2) Construct a new system block $S'$ by adding a site to $S$, similarly construct a new environment block $E'$.

(3) Construct the superblock of length $2l + 2$ from $S'$ and $E'$.

(4) Calculate the ground state $|\psi\rangle$ of the superblock Hamiltonian using exact diagonalization.

(5) Calculate the reduced density matrix $\hat{\rho} = Tr_E |\psi\rangle \langle\psi|$ and its eigenbasis $|\omega_\alpha\rangle$ arranged in descending order of its eigenvalues (weights) $\omega_\alpha$.

(7) Form a new truncated basis for $S'$ using $M^S$ eigenstates with the largest weights. Do the same thing for the environment.

(8) Re-write the Hamiltonian and all other operators for $S'$ in this new basis.

(9) Restart step (1) with block size $l + 1$ and repeat the process until the desired

length is reached.

Once the desired system size is reached, it is important to carry out the finite-system DMRG algorithm to increase the accuracy of the results, or in other words, to decrease the truncation error. All the steps of this procedure are similar to infinite-system DMRG except that in finite-system DMRG, the size of the lattice is kept fixed and one block grows in size while the other shrinks. When a block gradually increases (or decreases) in size, reaches some maximum (or minimum) and returns back to its original size, we call the process a sweep. The sweeping process is continued until the wavefunction and the energy are optimized, i.e., the more the sweeps, the more accurate the results. Figure 1.4.2 shows how the two algorithms work.

# Chapter 2

# Plane-polarized dipoles at half-filling

## 2.1 Motivation

The high degree of controllability offered by ultracold atoms and molecules in optical lattices has introduced many ideas to simulate interesting unsolved quantum models motivated by solid-state physics. In particular, low-dimensional systems in this context are of great interest, not only because of the recent development in creating real solid-state systems that can be described in theoretical models studied in the past, but also because an ultracold system may provide a test ground that is beyond the real material that we have access to today [71]. Moreover, many-body systems with long-range interactions are predicted to feature interesting quantum phases [1, 30, 31, 32]. In the presence of geometrical frustration, a situation where not all the interactions are satisfied, the system is expected to exhibit even more interesting features. For instance, quantum spin liquid phases have been found in frustrated spin−1 diamond antiferromagnets [72] and in frustrated spin−1/2 Heisenberg antiferromagnet on the kagome lattice [73]. Similarly, Haldane phases have been shown in a spin−1/2 frustrated ferromagnetic XXZ chain [74] and in a frustrated zigzag optical lattice

of ultracold bosons [75]. One of the questions that therefore arises is whether frustration in a zigzag lattice of plane-polarized dipoles leads to phases with non-trivial correlations between lattice points.

Over the years, there has been a lot of work to study the phase diagram of frustrated two-leg spin ladders using various models, for instance, Refs. [76, 77, 78, 79, 80]. As compared to those, our model is simple because it is one-dimensional, has fewer degrees of freedom, and still exhibits frustration.

Wang et. al. [71] showed a rich phase diagram for this system with the chain opening angle $\gamma \geq 2\pi/3$ (Figure 2.2.1a), a parameter regime with nearest-neighbor (NN) and next-nearest-neighbor (NNN) interactions, but only NN hopping. We produce a phase diagram for the same system, but setting NNN hopping to non-zero values, thus also allowing for much smaller chain opening angles $\gamma$. With the introduction of the NNN hopping, it becomes impossible to do exact calculations for a system size large enough to exhibit many-body effects, we therefore need a numerical approximation method. We use the Density Matrix Renormalization Group (DMRG) method [67, 68] because it is the most powerful numerical method available to simulate one-dimensional systems [70, 81, 82].

## 2.2 The model

Figure 2.2.1 shows the spin$-1/2$ representation of the zigzag chain of dipoles. A dipole at a site is represented by a spin up, $|1\rangle \equiv |\uparrow\rangle$, while an empty site is

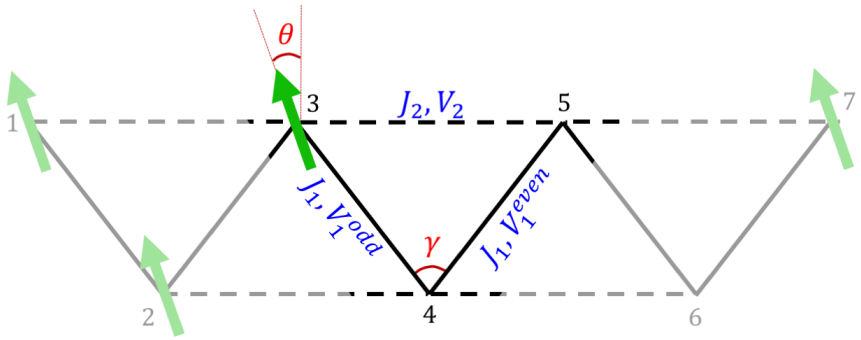


(a) Dipoles polarized at an angle $\theta$ in the plane of the zigzag chain

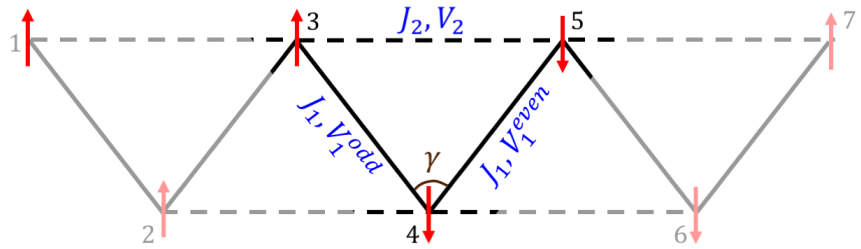


(b) Spin−1/2 particles replacing the dipoles

Figure 2.2.1: (Color online) A zigzag chain of dipoles mapped to one of spin−1/2 particles. For our DMRG simulations, we have considered $N = 100$ sites but the figure shows only seven sites labeled 1 through 7. The hopping is allowed in a leg/direction (odd, even or NNN) of the chain only if the ends of the leg contain opposite spins. Figures also appear in [83].

represented by a spin down, $|0\rangle \equiv |\downarrow\rangle$. With the constraint that double occupancy is not allowed on any lattice sites, we map this quasi-one-dimensional model of dipoles to a spin−1/2 chain. We treat these particles as hardcore bosons because two parallel dipoles on the same lattice site would experience an infinite on-site potential [71].

The Hamiltonian of the system is written as

$$\begin{aligned} H = &- J_1 \sum_j (S_j^+ S_{j+1}^- + h.c.) \; - \; J_2 \sum_j (S_j^+ S_{j+2}^- + h.c.) \\ &+ \; V_1^{odd} \sum_{j=odd} S_j^z S_{j+1}^z \; + \; V_1^{even} \sum_{j=even} S_j^z S_{j+1}^z \\ &+ \; V_2 \sum_j S_j^z S_{j+2}^z + \; h \sum_j S_j^z \end{aligned} \tag{2.2.1}$$

where $J_1 > 0$ and $J_2 > 0$ are NN and NNN hopping amplitudes and $h$ is the magnetic field. The system is half-filled, therefore the field term can be neglected. The spin operator $S^z$ is defined such that $S^z|\uparrow\rangle = |\uparrow\rangle$ and $S^z|\downarrow\rangle = -|\downarrow\rangle$. $V_1^{even}$ and $V_1^{odd}$ are NN dipolar interactions along even and odd legs of the chain respectively and $V_2$ is the NNN dipolar interaction. The interactions are related to the dipole coupling strength $\epsilon_{dd}$, chain opening angle $\gamma$ and polarization angle $\theta$ as [71]:

$$V_1^{even} = \epsilon_{dd}\left[1 - 3\cos^2\left(\pi - \frac{\gamma}{2} - \theta\right)\right] \tag{2.2.2}$$

$$V_1^{odd} = \epsilon_{dd}\left[1 - 3\cos^2\left(\frac{\gamma}{2} - \theta\right)\right] \tag{2.2.3}$$

$$V_2 = \frac{\epsilon_{dd}}{[2(1-\cos(\gamma))]^{3/2}}\left[1 - 3\cos^2\left(\frac{\pi}{2} - \theta\right)\right] \tag{2.2.4}$$

where $\epsilon_o$ and $\mu_e$ are the vacuum permittivity and electric dipole moment, and $\overrightarrow{r}_1$ and $\overrightarrow{r}_2$ are the position of the two interacting molecules. If $d_1$ and $d_2$ are the lengths of the odd (or even) and NNN legs, then $d_2 = 2\, d_1 \sin(\gamma/2)$.

Using this relation and the fact that the hopping amplitudes $J_1$ and $J_2$ decrease exponentially with distance, we can show that

$$\frac{J_2}{J_1} = \exp\Big[ - \frac{d_1}{\lambda}\Big(2\sin(\gamma/2) - 1\Big)\Big] \tag{2.2.5}$$

where $\lambda$ is a function of the lattice depth, and has the units of length. Although $d_1$ and $\lambda$ can change when $\gamma$ is varied, we can always set the ratio $d_1/\lambda$ to a desired value by tuning the lattice depth and thereby fixing $\lambda$ independent of $d_1$ or $\gamma$. The larger the value of the ratio $d_1/\lambda$, the deeper the lattice. Since $\gamma, \theta$ and $d_1/\lambda$ can be varied independently in real experiments, our model and all the results associated with it depend on these three parameters.

Before running any numerical simulations, we want to get an intuitive understanding of the model. We start with some fundamental questions: Is there any regime where we can predict the ground state of the system and then use numerics to validate our prediction? Can we identify the frustrated and non-frustrated regimes and map them to the physical parameter regime of $\gamma$ and $\theta$? How are the NN and NNN hopping amplitudes related to one another and to $\gamma$ and lattice depth? How different do the ground state phase diagrams look like for different lattice depths? As shown in Figure 2.2.1, there are pairwise interactions in odd, even and NNN directions, each of which can be attractive or repulsive. We will study the effect of each interaction separately and put

them together afterwards to analyze their collective effect on the system.

We write the Hamiltonian for any two interacting sites $i$ and $j$, where $j = i + 1$ or $i + 2$, as

$$H_{\text{two-site-term}} = \beta\left( -\frac{1}{2}(S_i^+ S_j^- + h.c.) + \alpha S_i^z S_j^z \right) \tag{2.2.6}$$

where $\beta = 2J$ and $\alpha = V/2J$, and we refer to them as "relative" hopping and interaction strengths respectively. If we exactly solve this "two site term" in the basis $\{|\uparrow\uparrow\rangle, |\uparrow\downarrow\rangle, |\downarrow\uparrow\rangle, |\downarrow\downarrow\rangle\}$, we will obtain the following result: Regardless of the value of $\beta$, the two sites prefer parallel alignment, $\uparrow\uparrow$ or $\downarrow\downarrow$ represented by the letter "F" (for "ferromagnetic") if the pairwise interaction $\alpha < -1/4$, and antiparallel alignment, $\uparrow\downarrow$ or $\downarrow\uparrow$ represented by the letter "A" (for "antiferromagnetic") if $\alpha > -1/4$. It is worth noting that the critical value $\alpha_c = -1/4$ lies at the boundary between the two different configurations.

We can rewrite the full Hamiltonian as

$$\begin{aligned} H = &\sum_{j=odd} \beta_1\left( -\frac{1}{2}(S_j^+ S_{j+1}^- + h.c.) + \alpha_o S_j^z S_{j+1}^z \right) \\ &+ \sum_{j=even} \beta_1\left( -\frac{1}{2}(S_j^+ S_{j+1}^- + h.c.) + \alpha_e S_j^z S_{j+1}^z \right) \\ &+ \sum_{j} \beta_2\left( -\frac{1}{2}(S_j^+ S_{j+2}^- + h.c.) + \alpha_2 S_j^z S_{j+2}^z \right) \end{aligned} \tag{2.2.7}$$

which is the sum of all the two-site terms in the three directions, where

$$\begin{aligned}\beta_1&=2J_1,\ \beta_2\ =\ 2J_2,\\ \alpha_o&=\frac{V_1^{odd}}{2J_1},\ \alpha_e\ =\ \frac{V_1^{even}}{2J_1},\ \alpha_2\ =\ \frac{V_2}{2J_2}.\end{aligned} \tag{2.2.8}$$

The Hamiltonian written in this form helps us identify the frustrated and non-frustrated regimes and predict the ground state of the system prior to any simulations as we will discuss in the next section.

Writing the hopping amplitudes $J_1$ and $J_2$ in terms of relative hopping amplitudes $\beta_1$ and $\beta_2$ in Eq. 2.2.5, we obtain

$$\frac{\beta_2}{\beta_1} = \exp\Big[-\frac{d_1}{\lambda}\big(2\sin(\gamma/2)-1\big)\Big] \tag{2.2.9}$$

Throughout this project, we use zero temperature, open boundary conditions, and $\epsilon_{dd} = 1$, and unless otherwise stated, $d_1/\lambda = 0.1$. In addition, we set $\beta_1 = 1$, and with this choice of $\beta_1$ we allow the interactions to be much stronger than the hopping. At this point, it should be noted that the Hamiltonian is a function of $\alpha$'s and $\beta$'s which depend on three independent parameters: $\gamma, \theta$ and $d_1/\lambda$. Figure 2.2.2 shows how $\beta_2$ varies with $\gamma$ for different lattice depths while Figure 2.2.3 illustrates how $\alpha_o, \alpha_e$ and $\alpha_2$ depend on $\gamma$ and $\theta$.

Before we proceed to the next section, we want to clarify that by setting the temperature to absolute zero we nullify thermal fluctuations. However, the

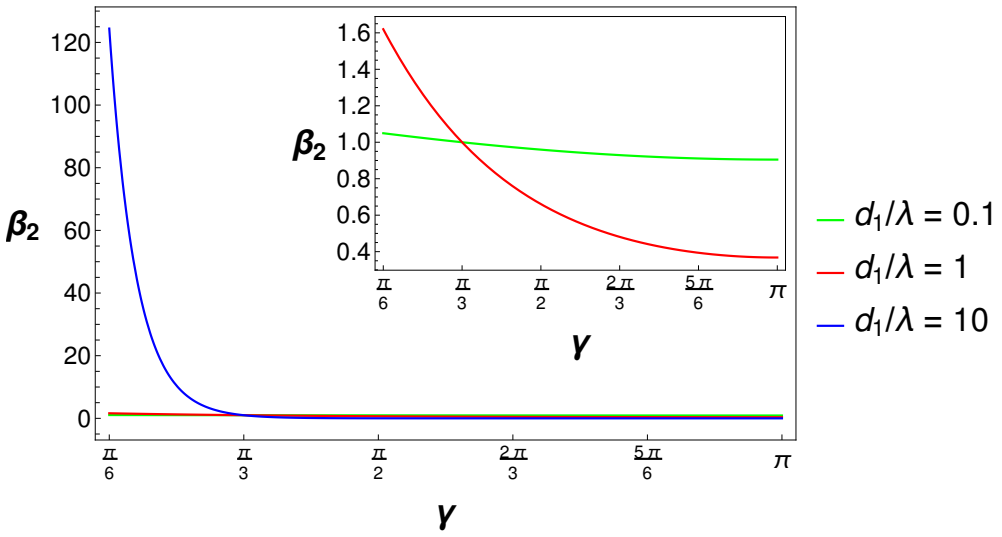


Figure 2.2.2: (Color online) Plot of $\beta_2$ against $\gamma$ for three different values of $d_1/\lambda$. Since $d_1/\lambda = 10$ corresponds to a deep lattice, $\beta_2$ increases much more exponentially with decreasing $\gamma$ as compared to the other two values of $d_1/\lambda$. The inset shows a zoomed in plot for $d_1/\lambda = 0.1$ which corresponds to a shallow lattice and for $d_1/\lambda = 1$ which corresponds to a lattice of intermediate depth as compared to the other two ratios. Figure also appears in [83].

experimental realization of this model would be a system at nanokelvin temperature with small but negligible thermal fluctuations. An example of such a system would be an ultracold bosonic gas of $^{23}Na^{87}Rb$ molecules that are stable against chemical reaction in their absolute ground state [84], have a large permanent electric dipole moment (for instance, as large as 3.3 Debye [85]) which can lead to strong dipolar interactions, and can be easily polarized by a moderate electric field. For instance, a 5 kV $cm^{-1}$ electric field can induce a dipole moment larger than 2 Debye [86]. As for the zigzag optical lattice, which can be produced by using three laser beams as explained in Ref. [87], it would be natural to set $d_1 \sim 1$ micrometer because lattice constant is typically of that order. With a dipole moment of 5 Debye (since experimentally realizable

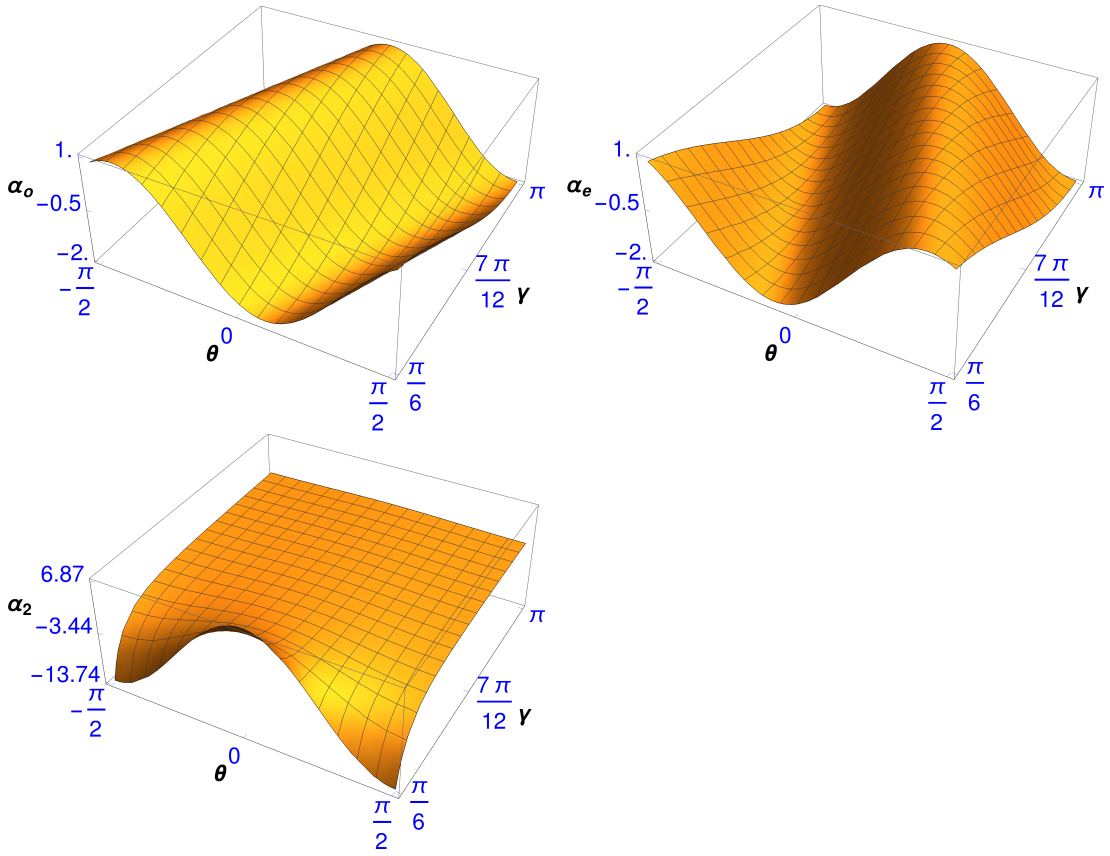


Figure 2.2.3: (Color online) Mapping of the relative interaction strengths $\alpha_o, \alpha_e$ and $\alpha_2$ to the physical parameter regime of the lattice, chain opening angle $\gamma$ and polarization angle $\theta$: Since $\beta_2$ and $\alpha_2$ diverge as $\gamma \to 0$, we take $\pi/6$ as an appropriate lower bound for $\gamma$. With $\pi/6 \leq \gamma \leq \pi$ and $-\pi/2 \leq \theta \leq \pi/2$, we observe that both $\alpha_o$ and $\alpha_e$ vary between $-2.00$ and $1.00$, while $\alpha_2$ varies between $-13.74$ and $6.87$. Figures also appear in [83].

systems consist of molecules with dipole moment $1 - 5$ Debye [88]), the dipolar coupling strength $\epsilon_{\rm dd} \approx \mu_e^2/4\pi\epsilon_o d_1^3 \approx 2.5 \times 10^{-30}$ Joules. A natural energy scale for molecules in optical lattice potentials is the molecular recoil energy $E_r = \hbar^2 k^2/2m$ where $m$ is the molecular mass. Since recoil energies (divided by the Plank constant $h$) are of the order of several kilohertz [89], we estimate that $E_r/h \sim 10$ kilohertz for molecular dipoles which means $E_r \approx 6.63 \times 10^{-30}$ Joules. With this estimate, we obtain $\epsilon_{dd} \approx 2.65 E_r$. By setting $\beta_1 = 1$ and $\epsilon_{dd} = 1$, we are

using $\epsilon_{dd}$ as our energy scale so that $J_1 = 0.5\epsilon_{dd}$, a value that might be too small to probe experimentally but could be increased by using smaller lattice constant (i.e., < 1 micrometer) or larger dipole moment (i.e., > 5 Debye). With this value of $J_1$, we can readily see how the interaction strength in each of the three directions scales with the corresponding hopping strength. For instance, when $(\gamma, \theta) = (\pi/3, \pi/3)$, we obtain $|J_1/V_1^{\text{even}}| = 0.5$, $|J_1/V_1^{\text{odd}}| = 0.4$ and $|J_2/V_2| = 0.4$.

## 2.3 Frustrated and non-frustrated regimes

In Figure 2.3.1, we saw how the eight regions - four frustrated (AAA, AFF, FAF and FFA) and four non-frustrated (FFF, AAF, AFA and FAA) - were related to the chain opening angle $\gamma$ and polarization angle $\theta$ given the ratio $d_1/\lambda = 0.1$. Figure 2.3.2 illustrates how these regions depend on the angles $\gamma$ and $\theta$ for other lattice depths. We find that all the eigght regions exist in our system, although their shape and size vary, regardless of the value of $d_1/\lambda$.

As mentioned in the previous section, the pairwise interaction $\alpha$ in any direction is attractive if $\alpha < -1/4$ or repulsive if $\alpha > -1/4$. If we arrange the interactions in all the directions based on whether they are attractive or repulsive, we find eight different combinations/regions as shown in Figure 2.3.1. Although this figure corresponds to the value of $d_1/\lambda = 0.1$, we get qualitatively similar plots for any other value of $d_1/\lambda$ as shown in Figure 2.3.2; this implies that the phase diagrams should also be similar regardless of the value of $d_1/\lambda$. Of the eight regions, four (AAA, AFF, FAF and FFA) are in the frustrated regime while the

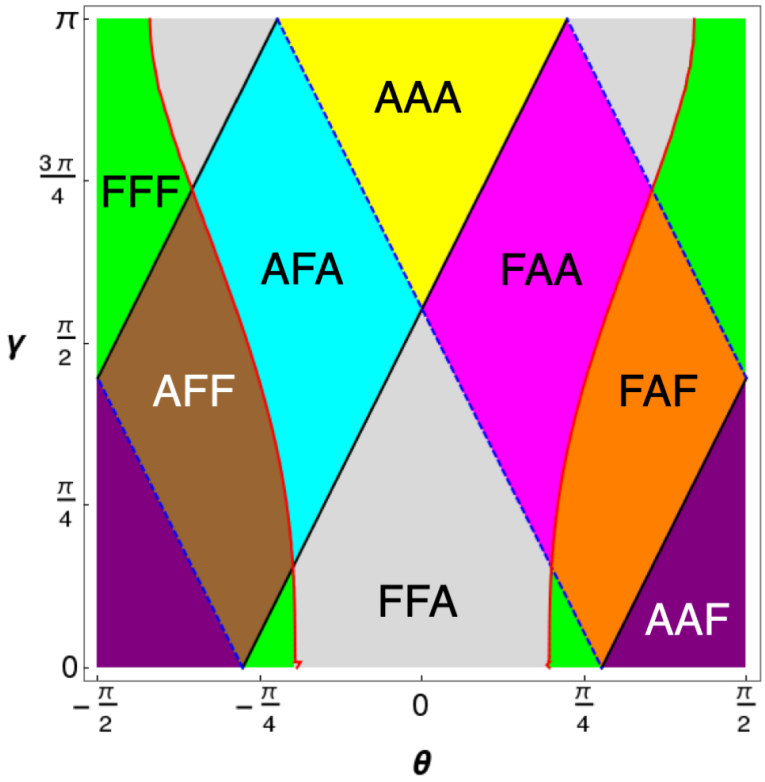


Figure 2.3.1: (Color online) Mapping of the frustrated and non-frustrated regimes to the physical parameter regime of chain opening angle $\gamma$ and polarization angle $\theta$. There are eight regions each with a unique color and labeled with three letters which correspond, from left to right, to the odd, even and NNN directions respectively (Frustrated: AAA, AFF, FAF and FFA; non-frustrated: FFF, AAF, AFA and FAA). The black solid, blue dashed and red solid lines represent the contours for $\alpha_o, \alpha_e$ and $\alpha_2$ respectively, each of which is equal to $-1/4$. Figure also appears in [83].

other four (FFF, AAF, AFA and FAA) are in the non-frustrated regime.

We will first explain and analyze non-frustrated regions in the absence of hopping and then discuss the potential scenario when the hopping is allowed. The simplest case of a non-frustrated regime is the region FFF where the pairwise interactions in all the directions are ferromagnetic (FM). In the absence of hopping, the spins would be classical and since the system is half-filled,

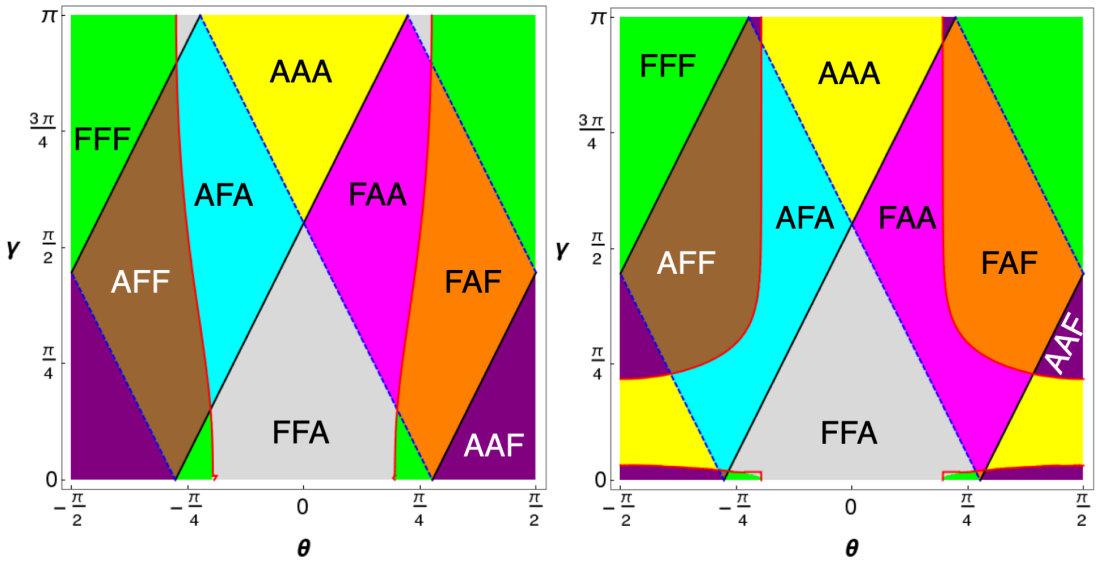


(a) $d_1/\lambda = 1$ (b) $d_1/\lambda = 10$

Figure 2.3.2: (Color online) Frustrated and non-frustrated regions for other lattice depths. Figures also appear in [83].

the two equal energy states $\{|\ldots\uparrow\uparrow\uparrow\downarrow\downarrow\downarrow\ldots\rangle, |\ldots\downarrow\downarrow\downarrow\uparrow\uparrow\uparrow\ldots\rangle\}$ would be the exact ground states (from now on, the curly braces {} will represent states with the same energy). Another non-frustrated region is AAF where the pairwise interactions in the odd and even directions prefer antiferromagnetic (AFM) alignment while that in the NNN direction prefers FM alignment. In the absence of hopping, the two Neel states $\{|\uparrow\downarrow\uparrow\downarrow\uparrow\downarrow\ldots\rangle, |\downarrow\uparrow\downarrow\uparrow\downarrow\uparrow\ldots\rangle\}$ are equally likely configurations to have the lowest energy and therefore, we expect the ground state to be AFM. Similarly, the ground state is expected to be a dimer of the type $\{|\uparrow\uparrow\downarrow\downarrow\uparrow\uparrow\downarrow\downarrow\ldots\rangle, |\downarrow\downarrow\uparrow\uparrow\downarrow\downarrow\uparrow\uparrow\ldots\rangle\}$ in the non-frustrated region FAA, and of the type $\{|\uparrow\downarrow\downarrow\uparrow\uparrow\downarrow\downarrow\ldots\rangle, |\downarrow\uparrow\uparrow\downarrow\downarrow\uparrow\uparrow\ldots\rangle\}$ in the non-frustrated region AFA. In the presence of hopping, however, the four non-frustrated regions could

feature phases that become superfluid instead of solid, particularly when the hopping dominates over the interactions.

The four regions in the frustrated regime are potentially more interesting. The first such region is AFF where the pairwise interaction in the odd leg prefers AFM alignment while those in the even and NNN legs prefer FM alignment. It is impossible for the spins to satisfy the interactions in all directions simultaneously, and hence the system is frustrated. We can make similar arguments to conclude that the other three regions FAF, FFA and AAA are also frustrated. As we will see later, there are regions in the frustrated regime where the pairwise interactions in the three directions are of similar strength and thus compete against one another. These regions require particular attention.

## 2.4 Phase diagram

Figure 2.4.1 shows the zero-temperature ground state phase diagram of the system for different values of $\gamma$ and $\theta$. This diagram has been produced with several DMRG trials each with a different initial state/condition, and the most appropriate ground state (the one with the lowest energy possible) has been considered. The different phases, the order parameters and correlation functions used to identify them, and the crossover between those phases will be discussed in the subsequent paragraphs. We label the initial state as $|\text{init}\rangle$. We name the initial state with spins randomly distributed in the lattice as "random initial state" and label it as $|\text{random}\rangle$. The letter "E" with a value attached to it

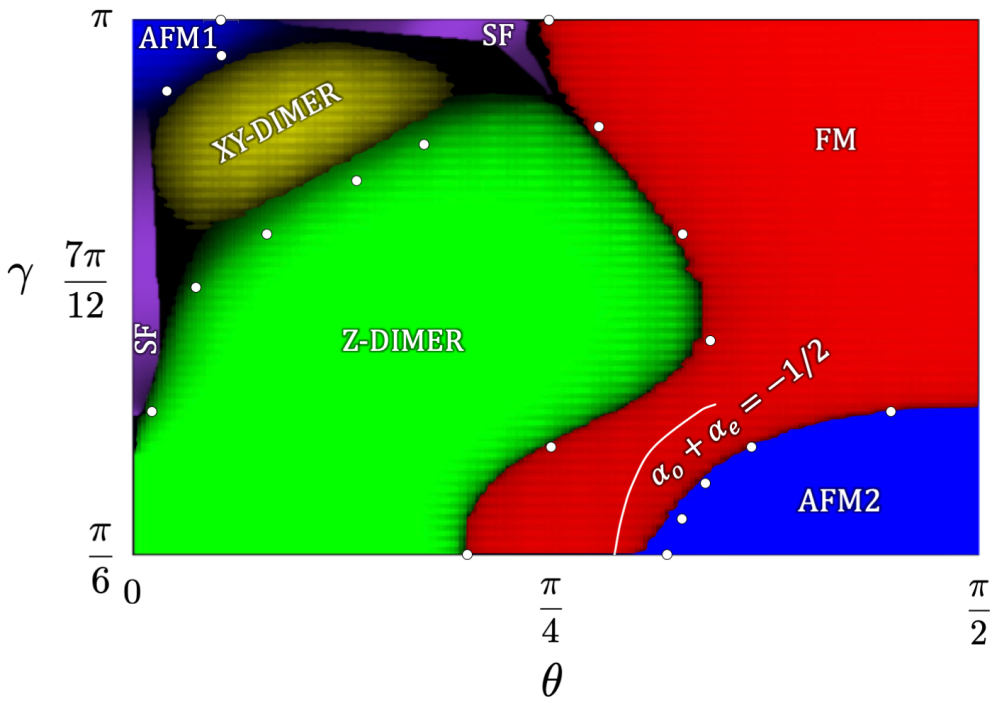


Figure 2.4.1: (Color online) Ground state phase diagram. These results depend on three independent parameters: chain opening angle $\gamma$, polarization angle $\theta$, and the ratio $d_1/\lambda$ which we have set equal to 0.1. Each color is associated with a different phase; the brighter a color, the deeper the system in that phase. The black color corresponds to the region where the order parameters vanish for all phases. AFM1 and AFM2 are both antiferromagnetic phases labeled differently because of the nature of the ground state returned by DMRG. The white curve labeled as "$\alpha_o + \alpha_e = -1/2$" represents the physical parameter regime where one of the pairwise interactions in NN directions is attractive while the other repulsive, and they both are the same distance away from their critical values $\alpha_{o,c} = \alpha_{e,c} = -1/4$. The superfluid phase has been drawn using the values of the correlation function for the finite system size $N = 100$. All the other phases and their boundaries have been drawn using the values of order parameters for the aforementioned system size. The white dots with very small error bars, obtained using finite-size scaling analysis, represent the phase boundaries in the thermodynamic limit $N \to \infty$. Figure also appears in [83].

will represent the energy of the ground state returned by a simulation. We will often show ground states for two different initial states to demonstrate how the initial conditions affect the final results obtained from DMRG simulations. When we show the results for only one initial state, it means that the state has

led to the most appropriate ground state. The color brightness for each phase represents the value of its order parameter while the black color represents the region where all the order parameters vanish. We produce this phase diagram for the finite system size $N = 100$ and we extrapolate the boundary between phases in the thermodynamic limit $N \to \infty$ using finite-size scaling analysis which we will discuss later. We find a sharp transition between FM and AFM phases, and hence DRMG pinpoints the boundary between these two phases, while we find a smooth transition everywhere else as we will discuss later.

It should be noted that the Hamiltonian Eq.(2.2.7) remains unchanged under the transformation $\theta \to -\theta$ (where $\alpha_o$ and $\alpha_e$ swap their values while $\alpha_2$ stays the same). This implies that the phase diagram gives similar results in the range $\theta \in [-\pi/2, 0]$ as in the range $\theta \in [0, \pi/2]$, and therefore, we can restrict ourselves to the latter.

### 2.4.1 Correlation functions

Before running the code, it is important to decide what quantities we want to measure and why. Since the Hamiltonian is written in terms of spin operators $S^+, S^-$ and $S^z$, it makes sense to calculate useful quantities, known as correlation functions, in terms of these operators. The ITensor library [90], the open-source package we have employed to implement DMRG, has easy-to-use pre-built functions that calculate these quantities. Here we want to explain what each of these correlation functions does. As we mentioned earlier, we have mapped

the dipoles to spin-1/2 particles such that a dipole at a site is spin up (↑) and an empty site is spin down (↓). If $\psi$ is the approximate ground state returned by DMRG, then with ITensor it is easy to calculate the quantities $\langle\psi| S^z_j |\psi\rangle$, $\langle\psi| S^z_j S^z_{j+1} |\psi\rangle$, $\langle\psi| S^z_1 S^z_j |\psi\rangle$, $\langle\psi| S^+_j S^-_j |\psi\rangle$ and $\langle\psi| S^+_1 S^-_j |\psi\rangle$, where $j$ is a lattice site under consideration. We embark to explain the physical meaning of these correlations with an example.

Suppose each of the two Neel states $\{|\uparrow\downarrow\uparrow\downarrow \ldots\rangle, |\downarrow\uparrow\downarrow\uparrow \ldots\rangle\}$ is equally likely to be the minimum energy configuration of the system. We say that the ground state is the superposition of these two states, the phase is known as antiferromagnetic which we will explain later in more details. The question is: What are expected values of the correlation functions that we discussed in previous paragraph? $\langle\psi| S^z_j |\psi\rangle$, or simply $\langle S^z_j\rangle$, for any given lattice site $j$ should yield a zero because since the ground state is a superposition of the two Neel states, if we measure the spin at the $j^{\text{th}}$ lattice site for a large number of times, for instance a million times, the site is spin up half of the time and spin down the other half. This is the definition of the expectation value such as $\langle S^z_j\rangle$ as found in common textbooks for quantum mechanics. However, as we will show later, DMRG could return one of the two Neel states as the ground state rather than a superposition and therefore, $\langle S^z_j\rangle = \pm 1$ when we expect $\langle S^z_j\rangle = 0$. Therefore, the calculation of $\langle S^z_j\rangle$ does not give us the whole picture. How about $\langle S^z_j S^z_{j+1}\rangle$? The physical meaning of this correlation is that if the spin at a given site is up (or down), $\langle S^z_j S^z_{j+1}\rangle = 1$ implies that the spin at its NN site is also up (or down) and $\langle S^z_j S^z_{j+1}\rangle = -1$

implies the spin at the NN site is down (or up). Similarly, $\langle S_1^z S_j^z \rangle = 1$ implies that the spins at the first and $j^{\text{th}}$ lattice sites are either both up or both down. Finally, the correlations $\langle S_j^+ S_{j+1}^- \rangle$ and $\langle S_1^+ S_j^- \rangle$ are used to measure if there is any exchange of spins between the two sites under consideration, and are therefore zero (or close to zero) for insulating phases as we will see later.

### 2.4.2 Z-dimer phase

In the earlier section, we mentioned two distinct sets of expected ground states: $\{|\uparrow\uparrow\downarrow\downarrow\uparrow\uparrow\downarrow\downarrow \ldots\rangle, |\downarrow\downarrow\uparrow\uparrow\downarrow\downarrow\uparrow\uparrow \ldots\rangle\}$ and $\{|\uparrow\downarrow\downarrow\uparrow\uparrow\downarrow\downarrow \ldots\rangle, |\downarrow\uparrow\uparrow\downarrow\downarrow\uparrow\uparrow \ldots\rangle\}$. We call this type of dimer a "z-dimer" and although the non-frustrated regions FAA and AFA are the natural candidates for this phase, a frustrated region can also exhibit this type of phase as shown in Figure 2.4.2.

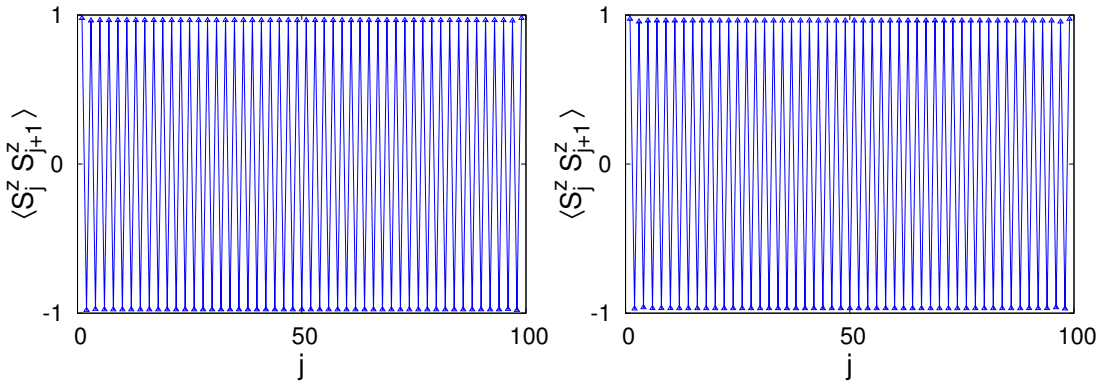


(a) $(\gamma, \theta) = (\pi/3, \pi/6)$. Region: FAA. (b) $(\gamma, \theta) = (\pi/3, \pi/12)$. Region: FFA.

Figure 2.4.2: (Color online) Z-dimer phase. $|\text{init}\rangle = |\downarrow\uparrow\downarrow\uparrow\downarrow\uparrow \ldots\rangle$. The left plot shows a z-dimer in the non-frustrated region FAA as expected. The right plot shows a similar phase in the frustrated region FFA which clearly indicates that the attractive interaction in the odd (or even) direction and the repulsive interaction in the NNN direction dominate over the attractive interaction in the third direction. Figures also appear in [83].

Figure 2.4.3 shows additional plots for the z-dimer phase shown in Figure 2.4.2a, which belongs to the non-frustrated region FAA. In principle, one should obtain $\langle S^z_j \rangle = 0$ for each site index $j$ because the ground state is expected to be a superposition of the two states $\{|\downarrow\downarrow\uparrow\uparrow\downarrow\downarrow\uparrow\uparrow \ldots\rangle, |\uparrow\uparrow\downarrow\downarrow\uparrow\uparrow\downarrow\downarrow \ldots\rangle\}$. However, DMRG returns one of these two states rather than a superposition. A similar argument is valid for all other phases. The other three plots are straightforward.

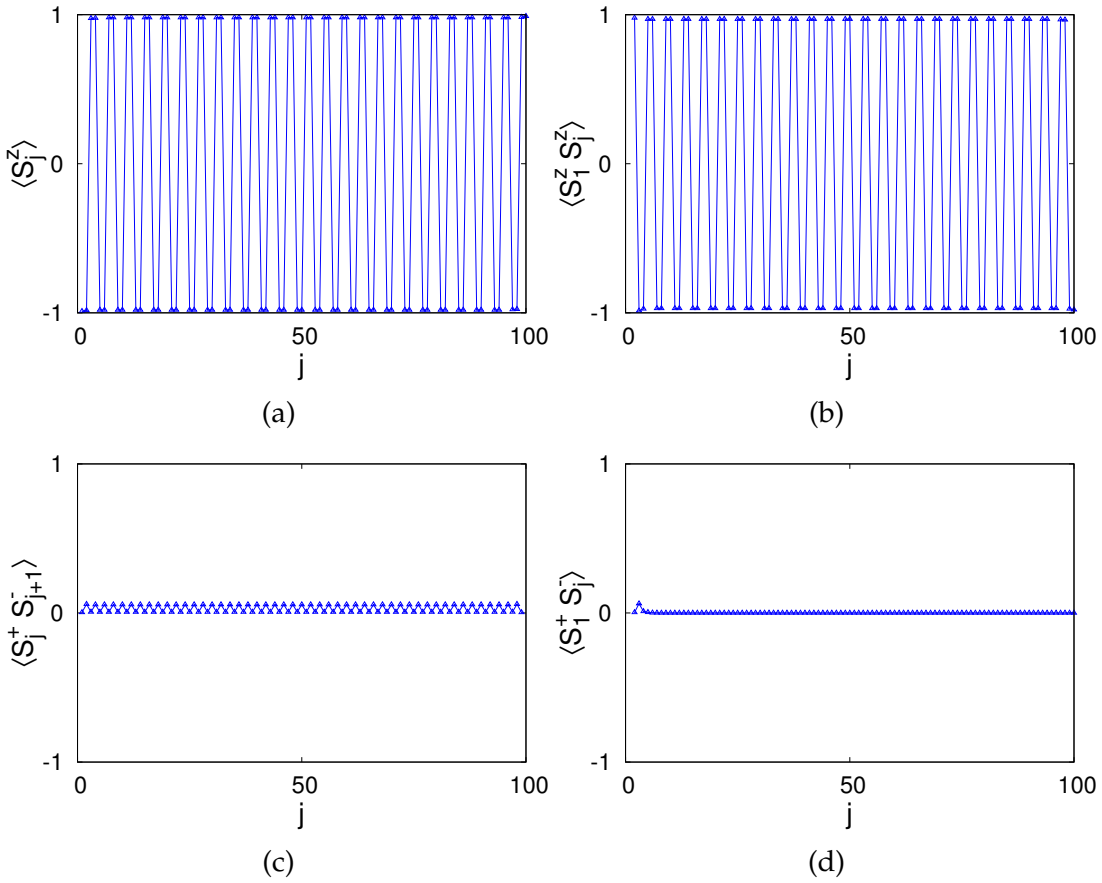


Figure 2.4.3: Additional correlations for the z-dimer phase. $(\gamma, \theta) = (\pi/3, \pi/6)$. $(\alpha_o, \alpha_e, \alpha_2) = (-2.000, 0.250, 0.250)$. Region: FAA. $|\text{init}\rangle = |\downarrow\uparrow\downarrow\uparrow\downarrow\uparrow \ldots\rangle$. Figures also appear in [83].

We would expect the same results regardless of whether the ground state is a single z-dimer state, as is the result from DMRG, or a superposition of two degenerate z-dimer states, as is the result from ab-intio calculations. A similar argument is valid for all other phases.

### 2.4.3 XY-dimer phase

Before discussing the other type of dimer that appears in the phase diagram, let us define $|+\rangle \equiv (1/\sqrt{2})(|\uparrow\downarrow\rangle + |\downarrow\uparrow\rangle)$. Then a "xy-dimer" is simply the triplet

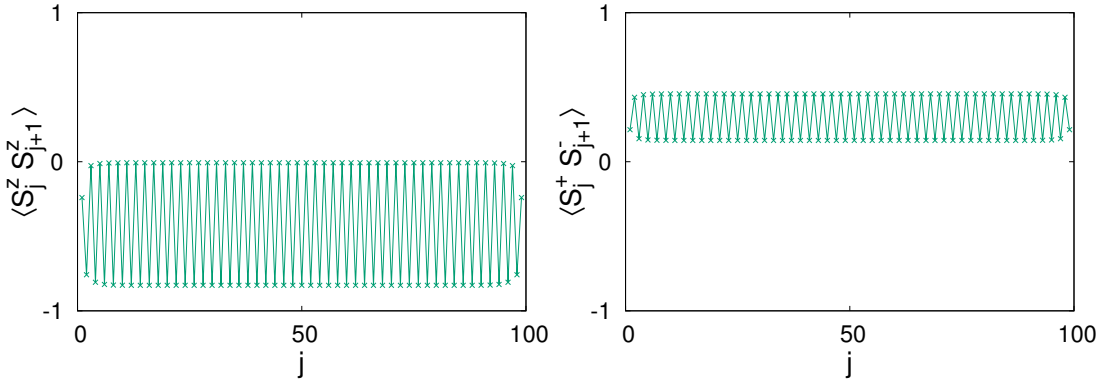


Figure 2.4.4: (Color online) XY-dimer phase. $(\gamma, \theta) = (5\pi/6, 0.0889\pi)$. Region: AAA. $|\text{init}\rangle = |\text{random}\rangle$. These two plots have been produced with exactly the same initial condition. What we see is an example of a xy-dimer with dangling spins, which means the repulsive interaction in the odd direction has a dominating effect over that in the even and NNN directions. Figures also appear in [83].

bound state $|+\rangle \otimes ... \otimes |+\rangle$ or the one with free spins at the edges (often referred to as "dangling spins") $\{|\uparrow\rangle \otimes |+\rangle \otimes ... \otimes |+\rangle \otimes |\downarrow\rangle, |\downarrow\rangle \otimes |+\rangle \otimes ... \otimes |+\rangle \otimes |\uparrow\rangle\}$. The xy-dimer with dangling spins (or bound spins at the edges) is plausible when the interaction in the even (or odd) direction is highly repulsive while that in the other two directions is weak as shown in Figure 2.4.4. If the hopping amplitudes were positive (i.e., $J_1 < 0$ and $J_2 < 0$), as is the case for fermionic statistics, the xy-triplets would be replaced with xy-singlets. It is worth noting that the xy-dimer with dangling spins will look similar to the valence bond solid state of the AKLT model if we replace the xy-triplets with xy-singlets; however, the absence of non-local correlation in the former makes it strikingly different from the latter.

Figure 2.4.5 shows additional plots for the xy-dimer phase shown in Figure

2.4.4.

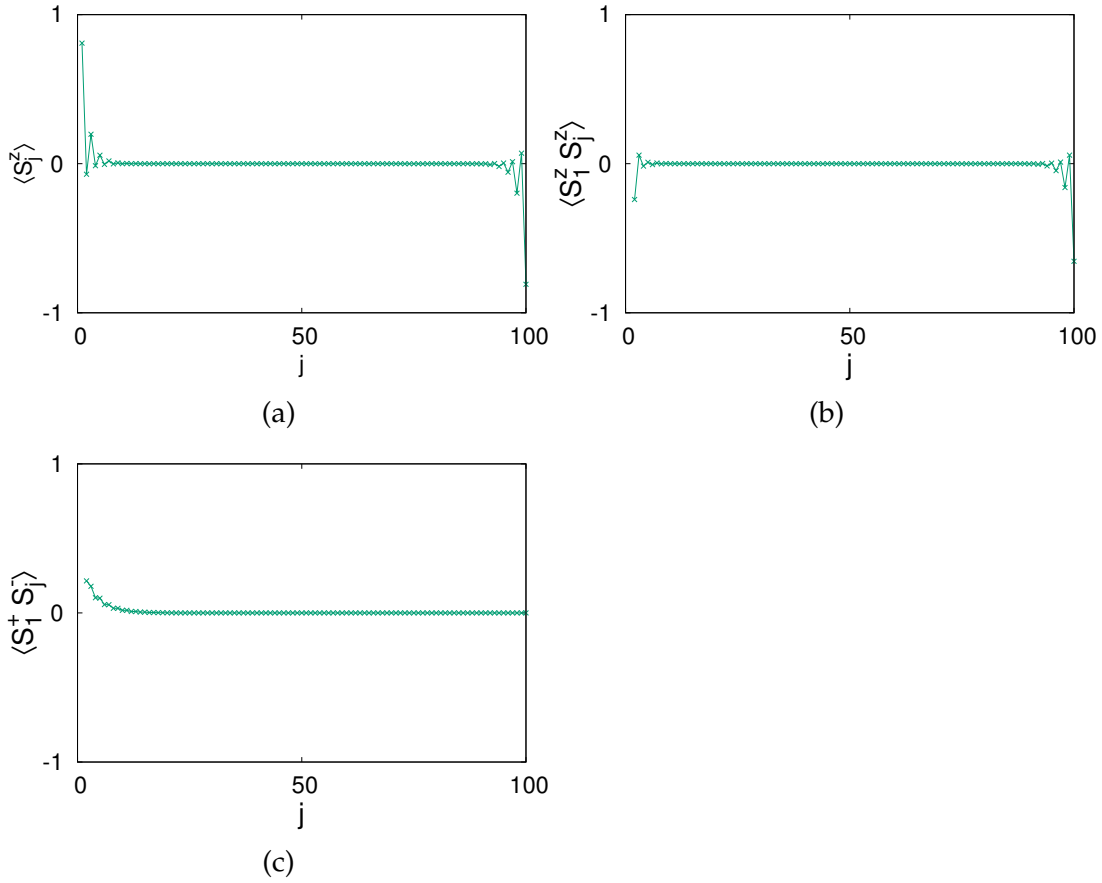


Figure 2.4.5: Additional correlations for the xy-dimer phase. $(\gamma, \theta) = (5\pi/6, 0.0889\pi)$. $(\alpha_o, \alpha_e, \alpha_2) = (0.204, 0.999, 0.117)$. Region: AAA. $|\text{init}\rangle = |\text{random}\rangle$. Figures also appear in [83].

For a finite lattice, a xy-dimer phase with bound spins at the edges is lower in energy than the one with dangling spins at the edges, and the system chooses as its ground state the former or the latter depending on the values of the pairwise interactions. In the thermodynamic limit, however, the two phases would have the same energy. Therefore, one would expect the frustrated region that results in the xy-dimer phase to be an ideal candidate for a spin liquid phase when the interactions in the odd and even directions are equally

repulsive; this would allow the ground state to be in the superposition of the two xy-dimer phases, a state similar to a *resonating valence bond* (see Ref. [91] for a nice review of this state) but with the xy-singlets replaced with xy-triplets. In other words, a spin liquid phase may occur if the triplet bond connecting two adjacent sites can freely switch between odd and even directions. The fact that the pairwise interactions in the two NN directions are always unequal in the xy-dimer regime of our model eliminates the possibility of a spin liquid phase.

Similarly, because of the existence of triplet bonds, the region in the phase diagram where a xy-dimer is observed is the only one where there could potentially be a Haldane phase. The existence of such a phase can be numerically investigated using a string correlation function [92, 93, 94, 95, 96, 97]. We consider the one employed by Furukawa et. al. [74]:

$$O^z_{\text{str}}(l, l+2r) = -\left\langle (S^z_l + S^z_{l+1}) \exp\left( i\pi \sum_{m=l+2}^{l+2r-1} S^z_m \right) (S^z_{l+2r} + S^z_{l+2r+1}) \right\rangle \tag{2.4.1}$$

To explain how this correlation function is associated with a Haldane phase, we consider a pair of spins at adjacent sites $l+2j$ and $l+2j+1$. If there were such a phase, the sum of the spins $S^z_{l+2j} + S^z_{l+2j+1}$ measured along the zigzag chain would alternate between $+1$ and $-1$ with one or more 0's in between, thus showing a hidden antiferromagnetic order. The correlation function $O^z_{\text{str}}(l, l+2r)$ would

detect this hidden order and take non-zero values as $r$ becomes large. We calculate this correlation function for all $j$ and $r$ but we do not see a pattern as explained before, and therefore we claim that we do not find a Haldane phase. And although we are unable to find one, we note that Xu et. al. [98] have shown the existence of such a phase in an experimentally realizable spin-1 model of bosons in a zigzag optical lattice.

### 2.4.4 Superfluid phase

By definition, superfluidity is the property of a fluid that moves with zero viscosity. In other words, there is no loss of kinetic energy when the constituents of the fluid move. A phase with this type of property is possible when the spins are not localized in lattice sites, and therefore it is expected in the frustrated regimes. The two plots in Figure 2.4.6 provide the evidence: A superfluid phase is found in the two frustrated regimes AAA and FFA.

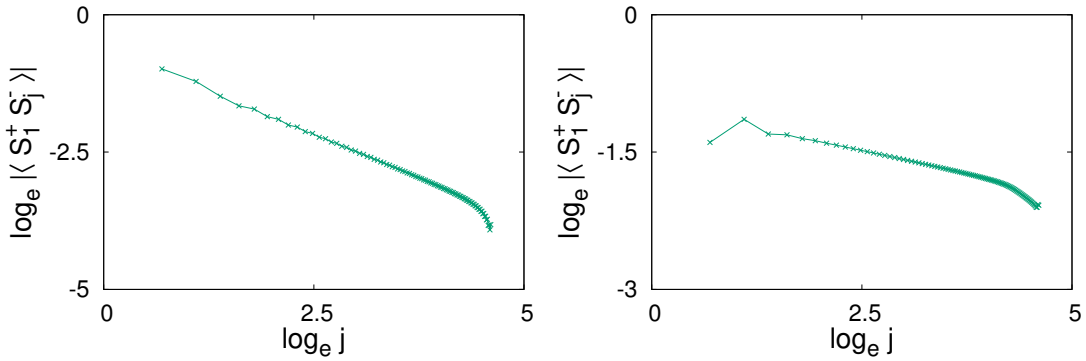


(a) $(\gamma, \theta) = (2\pi/3, 0)$. $(\alpha_o, \alpha_e, \alpha_2) = (0.250, 0.250, 0.207)$. Region: AAA.

(b) $(\gamma, \theta) = (\pi, 0.2333\pi)$. $(\alpha_o, \alpha_e, \alpha_2) = (-0.343, -0.343, -0.047)$. Region: FFA.

Figure 2.4.6: (Color online) SF phase. |init⟩ = |random⟩. The two plots show the polynomially decaying superfluid correlation; the non-polynomial decay near the open ends of the chain is due to the edge effect. Figures also appear in [83].

The reason that there are only small regions of superfluid (SF) phase in our phase diagram is that we choose our parameters such that the interactions are much stronger than the hopping. Depending on the values of $\beta_1$ and $\beta_2$, there can be various regions of SF phase. The existence of this phase is confirmed by the polynomially decaying long-range correlation $\langle S_1^+ S_j^- \rangle$ [99, 100], known as

the “superfluid correlation”, as shown in Figure 2.4.6.

These two plots also show that that the two different frustrated regions AAA and FFA can feature the same phase (SF in this case). It is worthwhile to look at the values of the pairwise interactions for the left plot: $(\alpha_o, \alpha_e, \alpha_2) = (0.250, 0.250, 0.207)$. While the interactions are equally repulsive in the NN directions, the one in the NNN direction is slightly less repulsive. This means the SF phase we observe is the result of the competition between the interactions in the three directions.

Figure 2.4.7 shows additional plots for the SF phase shown in Figure 2.4.6b, which belongs to the frustrated region FFA.

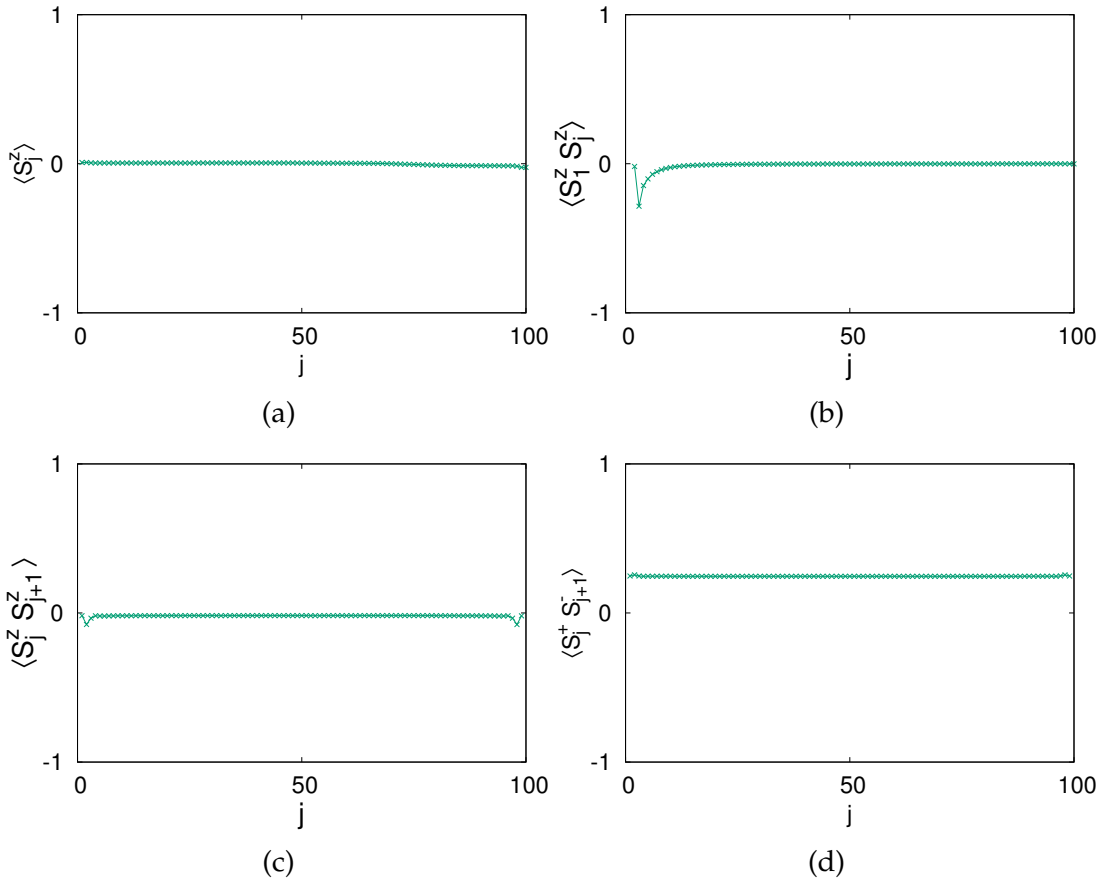


Figure 2.4.7: Additional correlations for the SF phase. $(\gamma, \theta) = (\pi, 0.2333\pi)$. $(\alpha_o, \alpha_e, \alpha_2) = (-0.343, -0.343, -0.047)$. Region: FFA. $|\text{init}\rangle = |\text{random}\rangle$. Figures also appear in [83].

### 2.4.5 Ferromagnetic phase

When the interactions in all the directions are attractive, hence the system in the non-frustrated region FFF, a ferromagnetic phase is expected which refers to the situation where one half of the spins on one side point in the downward direction while the other half point in the upward direction, or the other way round.

Figure 2.4.8 shows the ferromagnetic (FM) phase in this system. We show

results subject to two different initial conditions in order to highlight the nature of the phase returned by DMRG. When the system is in the FM regime, the FM state with a single domain wall is the true ground state because it has the lowest energy as compared to the states produced with any other initial conditions.

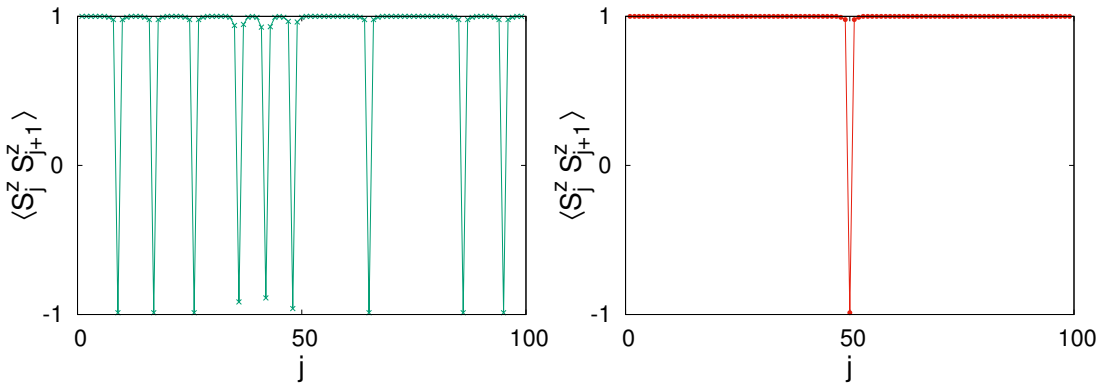


(a) $|\text{init}\rangle = |\text{random}\rangle$. $E = -178.26$. (b) $|\text{init}\rangle = |\ldots\downarrow\downarrow\downarrow\uparrow\uparrow\uparrow\ldots\rangle$. $E = -217.58$.

Figure 2.4.8: (Color online) FM phase. $(\gamma, \theta) = (\pi, \pi/2)$. $(\alpha_o, \alpha_e, \alpha_2) = (-2.000, -2.000, -0.276)$. Region: FFF. Since all the interactions are attractive at this point, the FM phase is expected unless the hopping dominates over the interactions. A single domain wall FM phase is the lowest energy state in this regime and the only way we can obtain this phase is by choosing itself as the initial condition. A simulation with any other initial state, although only the one with random initial state is shown here, results in a FM phase with several domain walls. Figures also appear in [83].

The dashed line on the phase diagram which is labeled as "$\alpha_o + \alpha_e = -1/2$" represents the points where $\alpha_o$ and $\alpha_e$ are equally far away from their critical values $\alpha_{o,c} = \alpha_{e,c} = -1/4$, one being attractive while the other repulsive. So one would expect a FM phase on one side of this line and an AFM phase on the other. Our results, however, show that the attractive interaction in the odd (or even) direction of the spin chain dominates over the repulsive interaction in the even (or odd) direction to a certain threshold, thus resulting in a FM phase

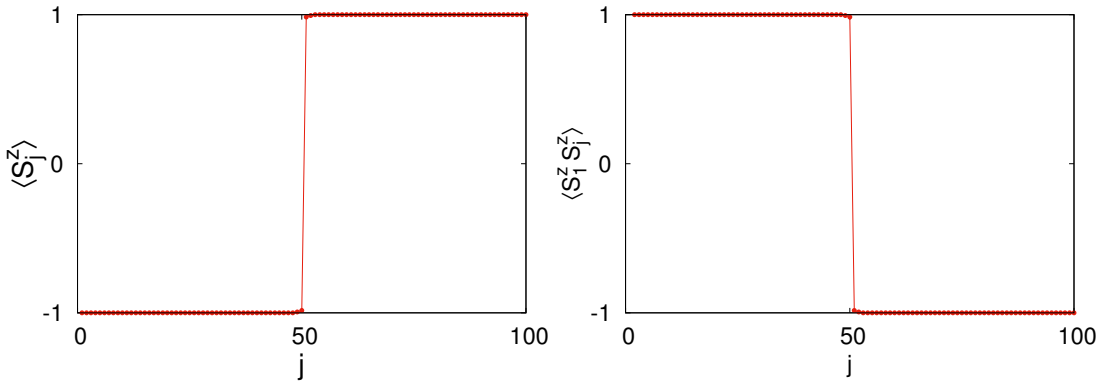


(a) (b)

Figure 2.4.9: (Color online) Additional correlations for the FM phase shown in Figure 2.4.8. $|\text{init}\rangle = |\ldots\downarrow\downarrow\downarrow\uparrow\uparrow\uparrow\ldots\rangle$. The values of the long-range correlation $\langle S_1^z S_j^z \rangle$ are as expected for a FM phase, while those of the correlation $\langle S_j^z \rangle$ suggest that DMRG returns one of the two FM ground states $\{|\ldots\downarrow\downarrow\downarrow\uparrow\uparrow\uparrow\ldots\rangle, |\ldots\uparrow\uparrow\uparrow\downarrow\downarrow\downarrow\ldots\rangle\}$. Figures also appear in [83].

on both sides of this line. It should be noted that this line disappears when $\gamma \to 0.4467\pi$ because above this value of $\gamma$, the system would be deep in the FM regime and therefore, we do not obtain an AFM phase regardless of the value of $\theta$.

Figure 2.4.9 shows the values of a couple of more correlation functions. The values of the correlation $\langle S_1^z S_j^z \rangle$ make sense. However, although we expect $\langle S_j^z \rangle = 0$ because the FM phase is the superposition of $\{|\ldots\downarrow\downarrow\downarrow\uparrow\uparrow\uparrow\ldots\rangle, |\ldots\uparrow\uparrow\uparrow\downarrow\downarrow\downarrow\ldots\rangle\}$, DMRG returns one of these two states rather than their superposition, and this is clear from the values of $\langle S_j^z \rangle$.

Figure 2.4.10 shows additional plots for the ferromagnetic phase shown in Figure 2.4.8. Both the correlation functions have negligible values because there is no exchange of spins in the lattice sites.

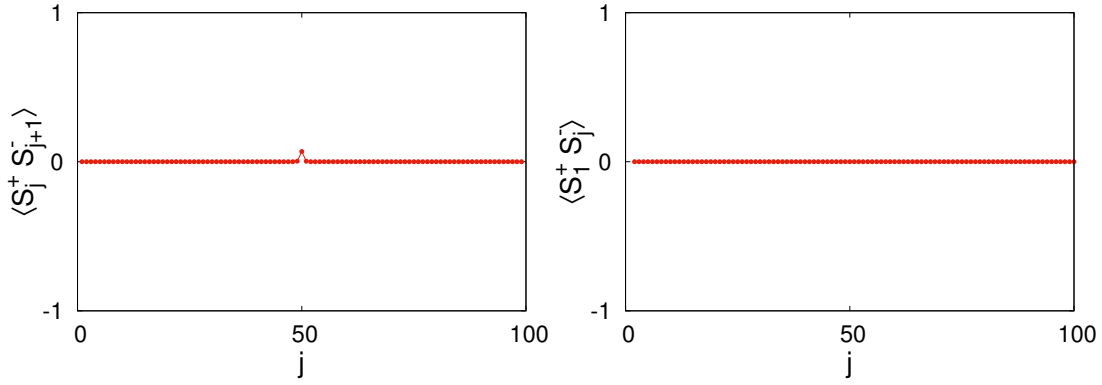


(a) (b)

Figure 2.4.10: Additional correlations for the FM phase. $(\gamma, \theta) = (\pi, \pi/2)$. $(\alpha_o, \alpha_e, \alpha_2) = (-2.000, -2.000, -0.276)$. Region: FFF. $|\text{init}\rangle = |\ldots\downarrow\downarrow\downarrow\uparrow\uparrow\uparrow\ldots\rangle$. Figures also appear in [83].

### 2.4.6 Antiferromagnetic phase

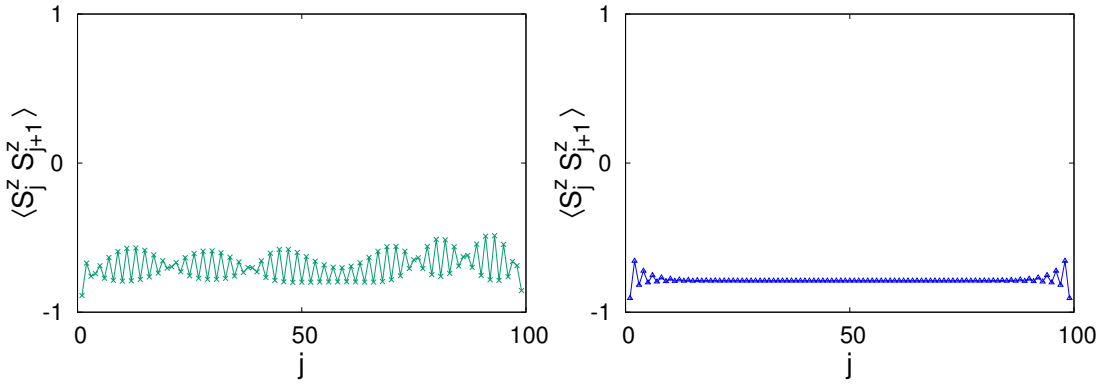


(a) $|\text{init}\rangle = |\text{random}\rangle$. $E = -96.13$. (b) $|\text{init}\rangle = |\downarrow\uparrow\downarrow\uparrow\downarrow\uparrow\ldots\rangle$. $E = -98.60$.

Figure 2.4.11: (Color online) AFM1 phase. $(\gamma, \theta) = (\pi, 0)$. Region: AAA. Although both the plots show an AFM phase, the one on the right is a better approximation to the true phase because it has a lower energy. Figures also appear in [83].

In Figure 2.4.11 and Figure 2.4.12, it can be seen that the accuracy of DMRG depends on the choice of initial state. There are obviously two different AFM regimes, and as mentioned earlier the AFM state is the superposition of the two

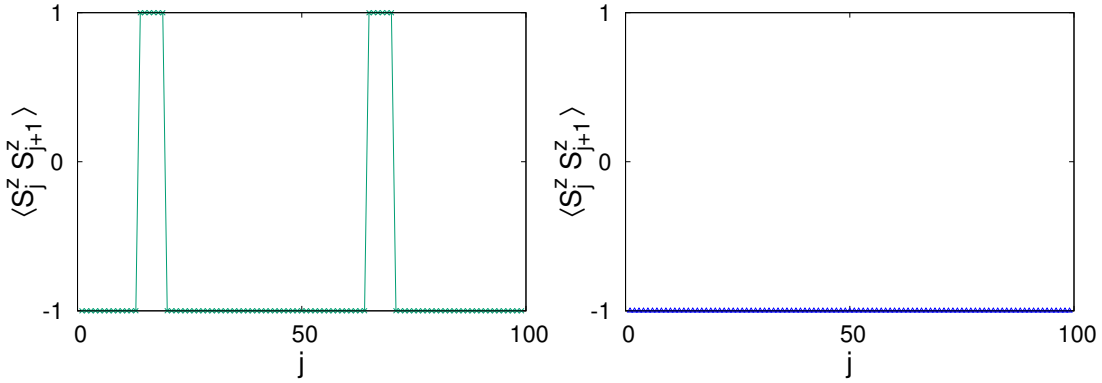


(a) $|\text{init}\rangle = |\text{random}\rangle$. $E = -1357.91$. (b) $|\text{init}\rangle = |{\downarrow}{\uparrow}{\downarrow}{\uparrow}{\downarrow}{\uparrow}\ldots\rangle$. $E = -1492.43$.

Figure 2.4.12: (Color online) AFM2 phase. $(\gamma, \theta) = (\pi/6, \pi/2)$. Region: AAF. The left plot shows a phase with mostly AFM correlations except for a couple of trapped regions while the right plot shows a pure AFM phase which is the true phase because it has a much lower energy. Figures also appear in [83].

Neel states. We label the phase as "AFM1" when the NN correlations $\langle S^z_j S^z_{j+1}\rangle$ are negative but less than -1 for each site index $j$ as shown in Figure 2.4.11. A look at the values of the long-range correlation $\langle S^z_1 S^z_j\rangle$ confirms that this is an AFM phase. Simlarly, we label the phase as "AFM2" when the system is deep in the AFM regime so that $\langle S^z_j S^z_{j+1}\rangle \approx -1$. It is worth noting that although a pure AFM phase is expected in the non-frustrated region AAF, a simulation with a random initial state results in a phase that has mostly AFM correlations but with one or more clusters of identical spins, which we call "trapped regions". It is clearly not a true phase but still makes sense from an experimental point of view, which we will explain later.

Figures 2.4.13 and 2.4.14 show the additional plots for the AFM1 and AFM2 phases shown in Figures 2.4.11 and 2.4.12 respectively.

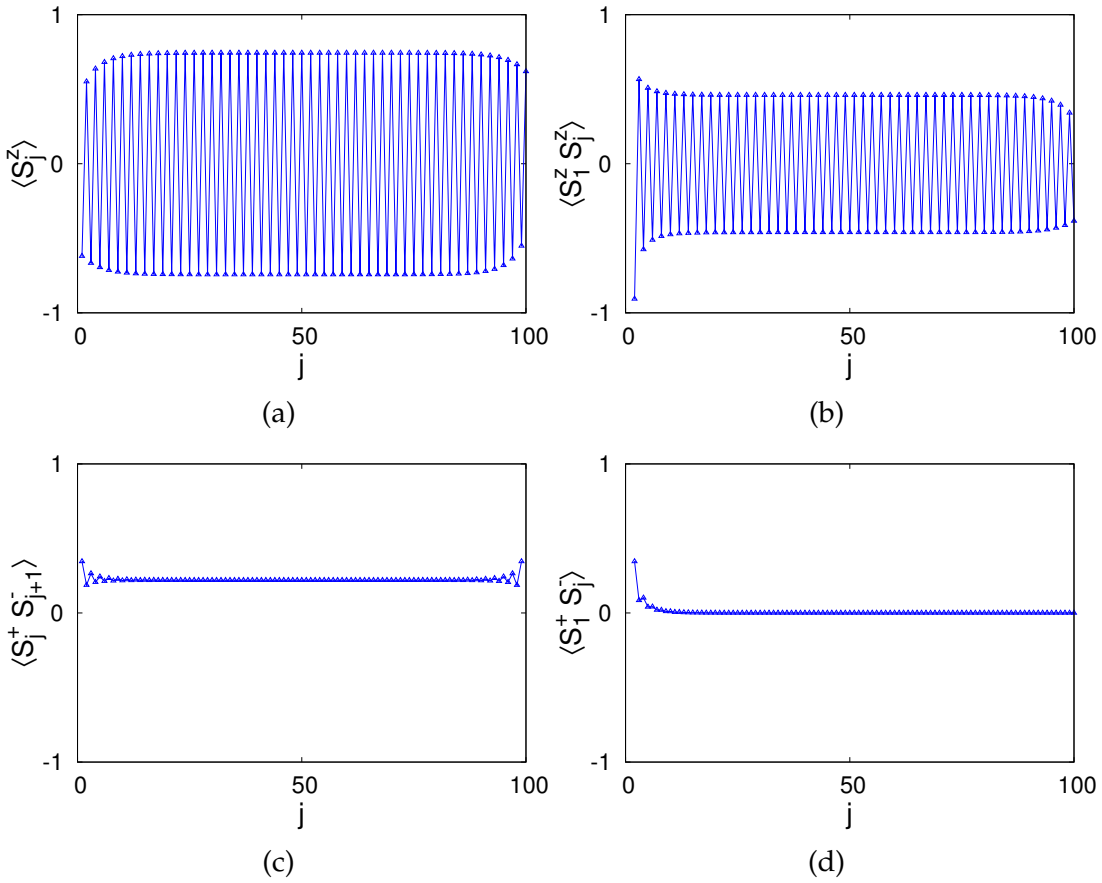


Figure 2.4.13: Additional correlations for the AFM1 phase. $(\gamma, \theta) = (\pi, 0)$. $(\alpha_o, \alpha_e, \alpha_2) = (1.000, 1.000, 0.138)$. Region: AAA. $|\text{init}\rangle = |{\downarrow}{\uparrow}{\downarrow}{\uparrow}{\downarrow}{\uparrow}\ldots\rangle$. Figures also appear in [83].

### 2.4.7 Phase transitions and DMRG

Figure 2.4.15 shows how initial states affect the ground state energy in DMRG simulations and why it is important to perform multiple trials with various initial conditions. If we look at these results with reference to the phase diagram (Figure 2.4.1), we can see that in the regime where the ground state is expected to be dimerized or AFM, the best choice for the initial state would be a z-dimer, a Neel state or a xy-dimer because these three states result in exactly the same

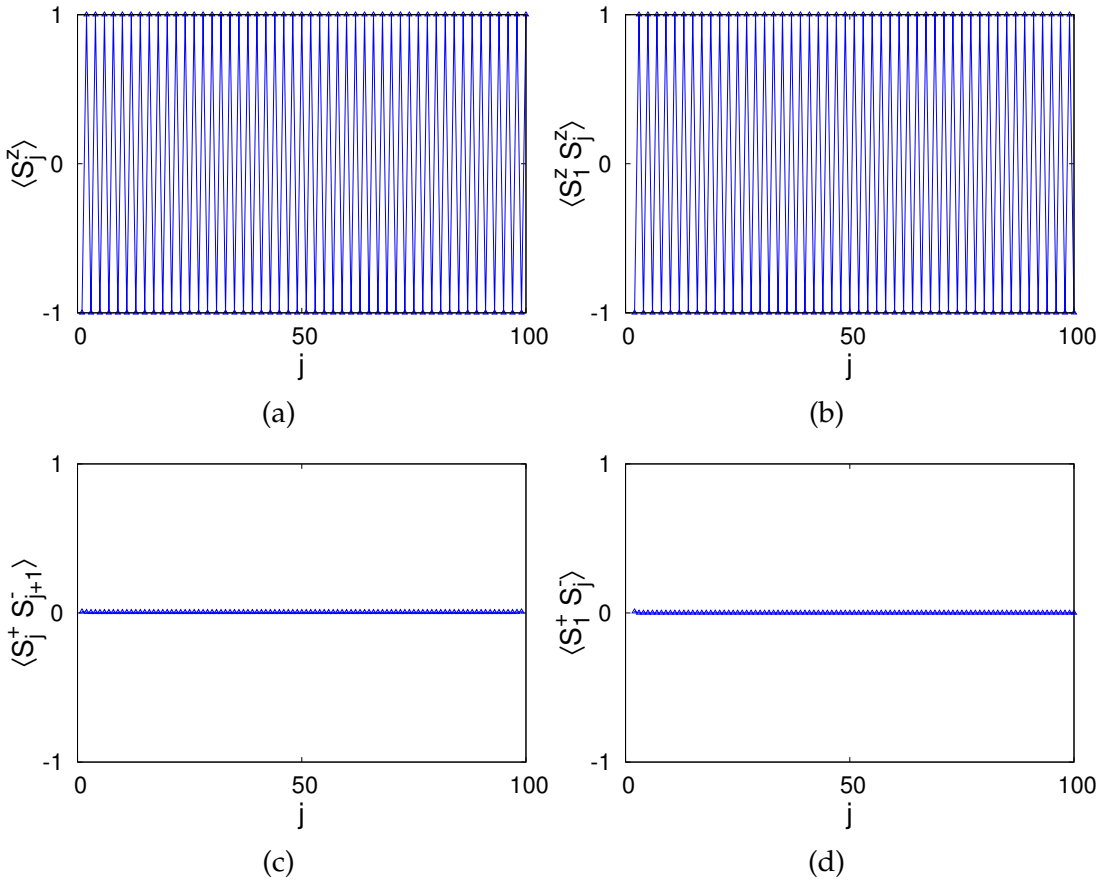


Figure 2.4.14: Additional correlations for the AFM2 phase. $(\gamma, \theta) = (\pi/6, \pi/2)$. $(\alpha_o, \alpha_e, \alpha_2) = (0.799, 0.799, -13.740)$. Region: AAF. $|\text{init}\rangle = |\downarrow\uparrow\downarrow\uparrow\downarrow\uparrow \ldots\rangle$. Figures also appear in [83].

ground state. Similarly, in the regime where the ground state is expected to be FM, a simulation must start with a single domain wall FM state.

Simulations with various initial conditions clearly show that there is a sharp transition between FM and AFM phases, and a smooth transition between z-dimer and FM phases and between SF and other phases. We will explain the transition between SF and AFM phases in more details later. Experiments, however, can be expected to confirm the unclear DMRG results in the following way: Suppose we build a system from a sample of randomly distributed spins

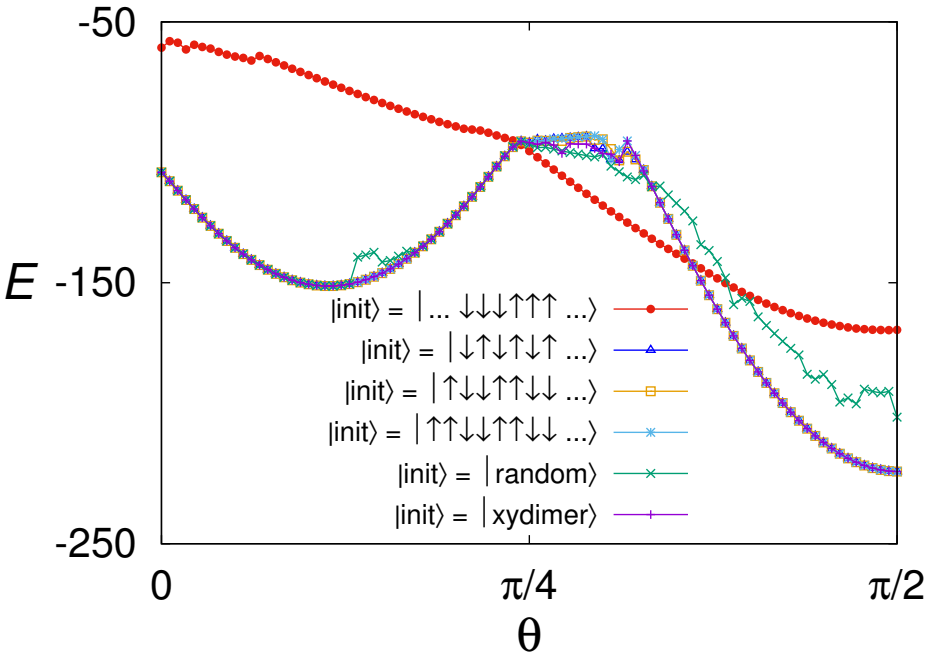


Figure 2.4.15: (Color online) Ground state energy of the system, $E$, plotted as a function of polarization angle, $\theta$, for $\gamma = \pi/3$. The state $|\text{init}\rangle$ has been used to denote the "initial state" for a DMRG simulation, $|\text{random}\rangle$ denotes the "random initial state" and $|\text{xydimer}\rangle$ denotes the triplet bound state $|+\rangle \otimes \ldots \otimes |+\rangle$. This figure shows that several curves meet at two points: $\theta = 0.2424\pi$, which belongs to a smooth crossover between z-dimer and FM phases (see Figure 2.4.16), and $\theta = 0.3598\pi$, which lies at a sharp crossover between FM and AFM phases (see Figure 2.4.17). When $0.2424\pi \leq \theta \leq 0.3598\pi$, the true ground state is FM which can only be obtained through a simulation with a FM initial state as shown here. Figure also appears in [83].

and slowly cool it down so that the spins restribute in the lattice to minimize their energy. If the sample consists of one or more trapped regions, the system must overcome an enormous energy hurdle to flip the spins in these regions, therefore the spin configuration would be expected to show signatures of these trapped regions (as we saw earlier in Figure 2.4.12) although it is not the lowest energy configuration.

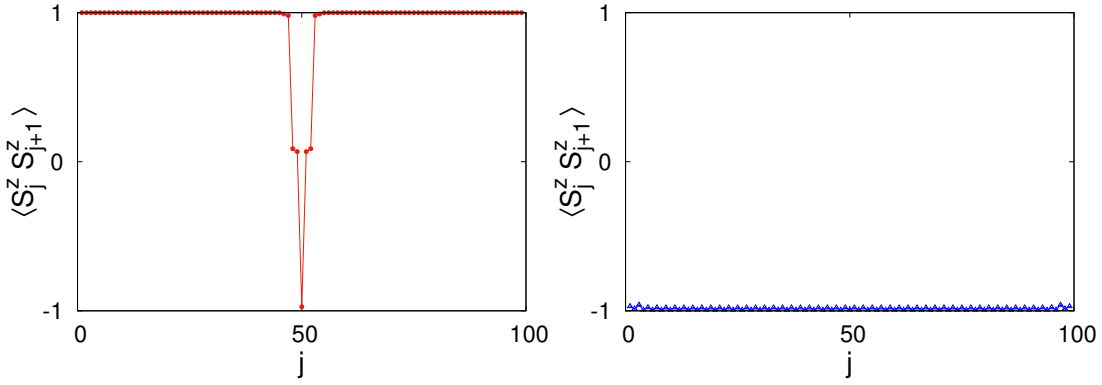


(a) $|\text{init}\rangle = |\ldots \downarrow\downarrow\downarrow\uparrow\uparrow\uparrow \ldots\rangle$. $E = -142.14$. (b) $|\text{init}\rangle = |\downarrow\uparrow\downarrow\uparrow\downarrow\uparrow \ldots\rangle$. $E = -142.13$.

Figure 2.4.16: (Color online) Ground states and their energies subject to two initial conditions. $(\gamma, \theta) = (\pi/3, 0.3598\pi)$. Region: FAF. Figures also appear in [83].

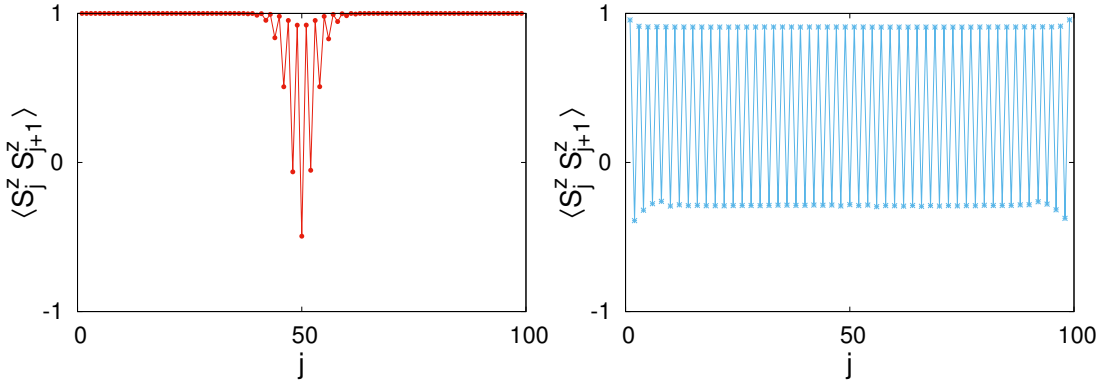


(a) $|\text{init}\rangle = |\ldots \downarrow\downarrow\downarrow\uparrow\uparrow\uparrow \ldots\rangle$. $E = -96.31$. (b) $|\text{init}\rangle = |\uparrow\uparrow\downarrow\downarrow\uparrow\uparrow\downarrow\downarrow \ldots\rangle$. $E = -96.30$.

Figure 2.4.17: (Color online) Ground states and their energies subject to two initial conditions. $(\gamma, \theta) = (\pi/3, 0.2424\pi)$. Region: FAF. Figures also appear in [83].

### 2.4.8 Transition between antiferromagnetic and superfluid phases

In the phase diagram, it is hard to locate the exact boundary between AFM and SF phases for the finite system size $N = 100$. To understand the transition between these two phases, we neglect the hopping and interaction in the NNN direction (i.e., we set $\beta_2 = 0$ and $\alpha_2 = 0$.). We are interested in the situation

where $\alpha_{o,e} > -1/4$, which means the pairwise interactions prefer antiparallel alignment of spins. As before, we set $\beta_1 = 1$ and for convenience, we consider $\alpha_o = \alpha_e$.

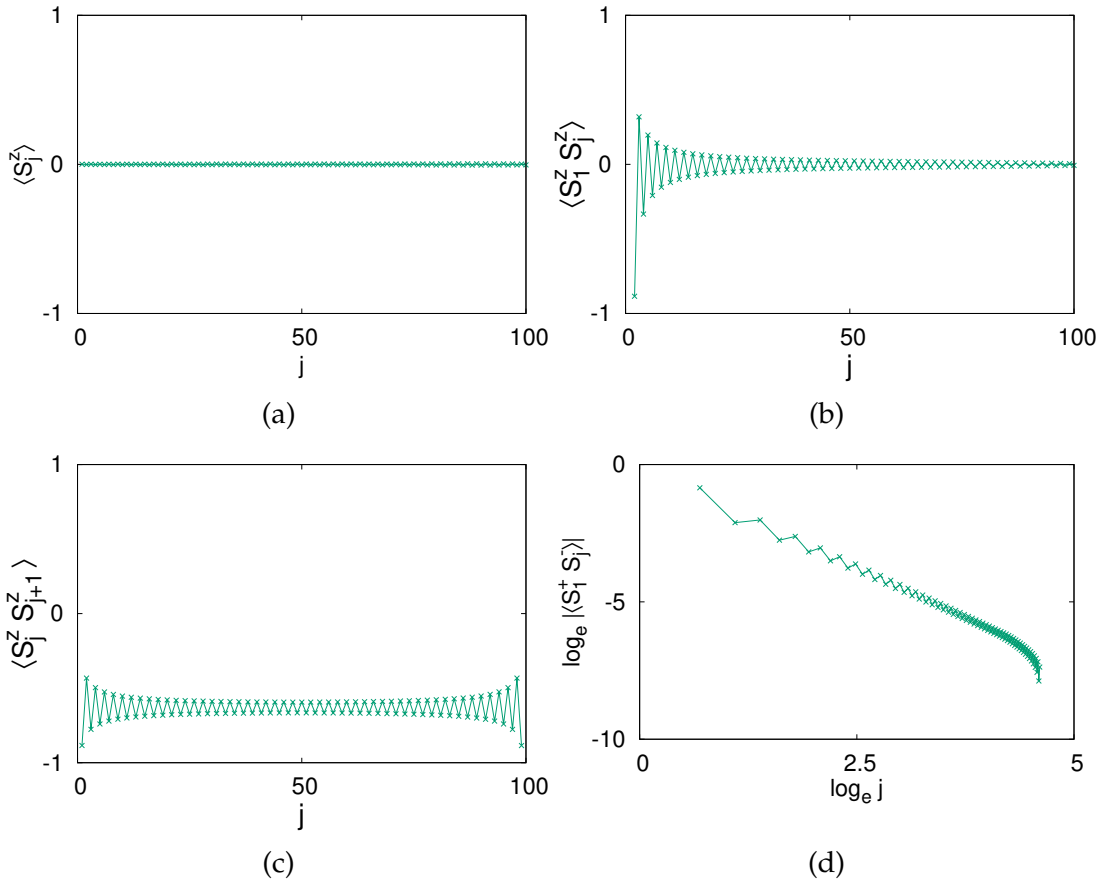


Figure 2.4.18: Correlations for the SF phase with $\beta_1 = 1, \alpha_o = \alpha_e = 0.3$. $|\text{init}\rangle = |\text{random}\rangle$. Figures also appear in [83].

Figure 2.4.18 and Figure 2.4.19 show the various correlations for the cases $\alpha_{o,e} = 0.3$ and $\alpha_{o,e} = 0.4$. It is interesting to note that the nature of the correlations $\langle S_j^z S_{j+1}^z \rangle$ and $\langle S_1^z S_j^z \rangle$ is not very different for the two cases; in fact, these correlations suggest the likelihood of an AFM phase. However, a SF phase in the former case is confirmed by the polynomial decay of the correlation $\langle S_1^+ S_j^- \rangle$

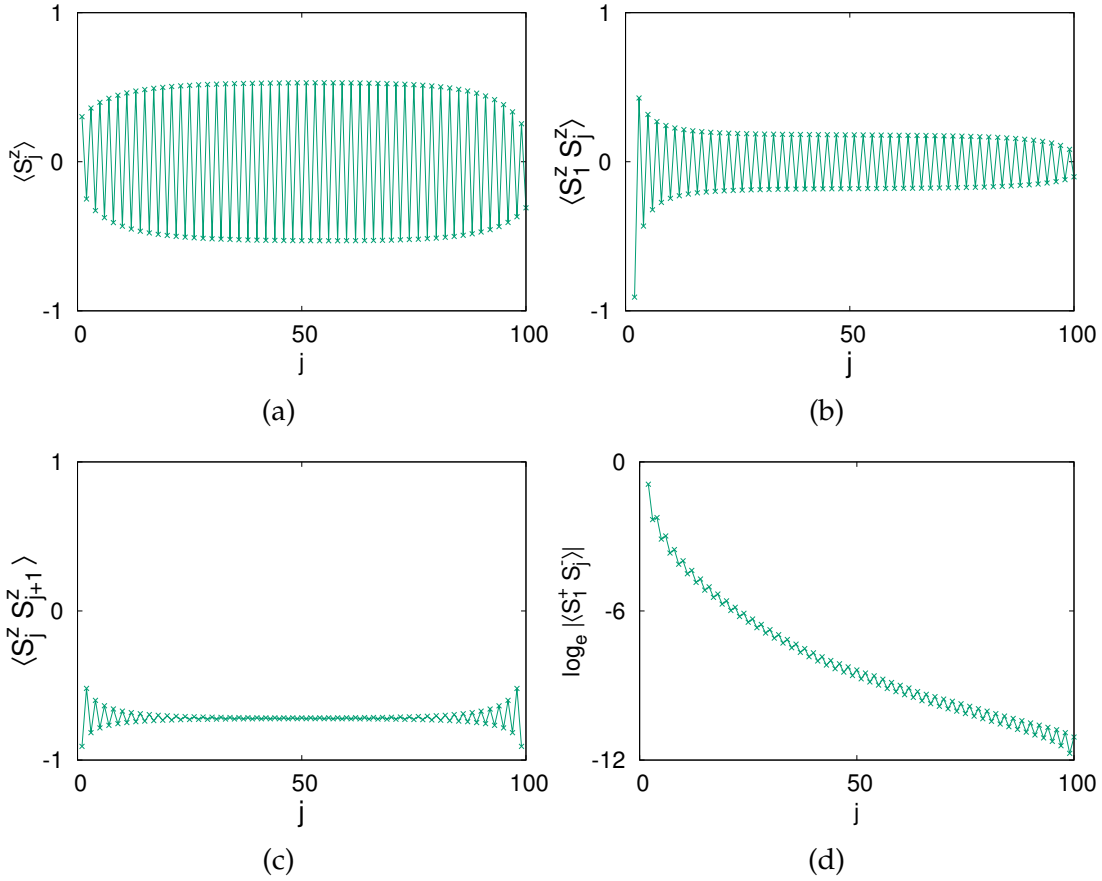


Figure 2.4.19: Correlations for the AFM phase with $\beta_1 = 1, \alpha_o = \alpha_e = 0.4$. |init⟩ = |random⟩. Figures also appear in [83].

while an AFM phase in the latter is confirmed by the tendency of the spins to localize in lattice sites as indicated by the alternating sign for the values of the correlation $\langle S_j^z \rangle$ and the exponential decay of the correlation $\langle S_1^+ S_j^- \rangle$ which clearly indicates an insulating phase.

Therefore, depending on the strength of $\beta_1$ (with hopping and interaction between nearest-neighbors only), the system can be in a SF or AFM phase when the pairwise interactions in the odd and even directions prefer antiparallel alignment. We also notice that there is a smooth crossover somewhere be-

tween $\alpha_{o,e} = 0.3$ and $\alpha_{o,e} = 0.4$. Based on these results, it is safe to conclude that the nature of the transition between SF and AFM phases in the phase diagram (Figure 2.4.1) is qualitatively the same.

### 2.4.9 Order parameters

We define the order parameters for ferromagnetic, antiferromagnetic, z-dimer and xy-dimer phases as follows:

$$O_{\text{ferro}} = \frac{4}{N} \sum_{i=\frac{N}{4}+1}^{\frac{N}{2}} \left| \sum_{j=\frac{3N}{4}}^{\frac{3N}{4}+3} \langle S_i^z S_j^z \rangle \right| \tag{2.4.2}$$

$$O_{\text{neel}} = \frac{4}{N} \sum_{i=\frac{N}{4}+1}^{\frac{N}{2}} \left| \sum_{j=\frac{3N}{4}}^{\frac{3N}{4}+3} (-1)^j \langle S_i^z S_j^z \rangle \right| \tag{2.4.3}$$

$$O_{\text{zdimer}} = \frac{2}{N} \sum_{i=\frac{N}{4}+1}^{\frac{3N}{4}} \left| \langle S_i^z S_{i+1}^z - S_{i+1}^z S_{i+2}^z \rangle \right| \tag{2.4.4}$$

$$O_{pxrxydimer} = \left| \sum_{i=\frac{N}{4}+1}^{\frac{N}{4}+4} (-1)^i \left| \langle S_i^z S_{i+1}^z \rangle \right| \right| \tag{2.4.5}$$

Although we use correlation functions to explain how we identify each phase, we use order parameters to find how deep the system is in a given phase and also to find the crossover between the phases. For the dimerized phases, we use

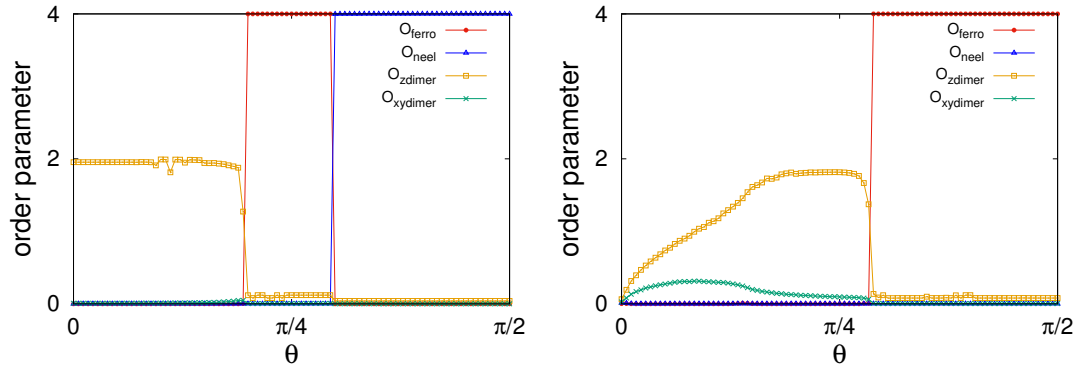


(a) $\gamma = \pi/6$ (b) $\gamma = 7\pi/9$

Figure 2.4.20: Order parameter for various phases as a function of polarization angle $\theta$. Figures also appear in [83].

the definitions given by Furukawa et. al.[74] To minimize the edge effects due to open boundaries, we use the method employed by Rossini et. al.[99] – we define the order parameters for ferromagnetic, antiferromagnetic and z-dimer phases as average expectation values of the correlators between spins in the middle part of the chain. For the xy-dimer phase, however, we only consider the the correlations $N/4$ sites away from the left end of the chain but not their average expectation values. For the superfluid phase, we use the values of the superfluid correlation function $\langle S_1^+ S_j^- \rangle$ which, as mentioned earlier, decays polynomially in this phase. It should be noted that we have defined the order parameters such that they are always non-negative.

Figure 2.4.20 shows how the order parameters for different phases vary with polarization angle $\theta$ for a given value of $\gamma$. By definition, the order parameter for a given phase should vanish in all other phases and our results for FM and AFM phases are consistent with this. However, the dimerized phases consist

of two flavors, xy and z, which pair neighboring spins in different directions. Therefore, their order parameters overlap. The finite size scaling, which we will discuss later, along with the values of correlation functions allows us to find the boundary between these two phases.

### 2.4.10 Finite-size scaling

As mentioned earlier, the phase diagram (Figure 2.4.1) has been drawn using the values of order parameters and correlation functions for the finite system size $N = 100$. We extrapolate the phase boundaries in the thermodynamic limit $N \to \infty$ using the finite-size scaling method explored by Rossini et. al. [99] We calculate the energy gap for different system sizes $N$ and find the value of $\theta$ for which the gap is minimum for each $N$, as shown in Figure 2.4.21a. We call this value $\theta_{pxrmin}$. We then plot these $\theta_{pxrmin}$ against $1/N$ and extrapolate the value of $\theta_{\text{min}}$ when $1/N \to 0$ as shown in Figure 2.4.21c. Although difficult to see, the boundaries denoted by white dots in the phase diagram have small error bars that are due to uncertainty in the fitting of the curves for different values of $N$. Our analysis shows that the energy gap scales polynomially with the system size near the boundary between z-dimer and ferromagnetic phases as shown in Figure 2.4.21b. We are unable to find the boundary between xy-dimer and superfluid phases.

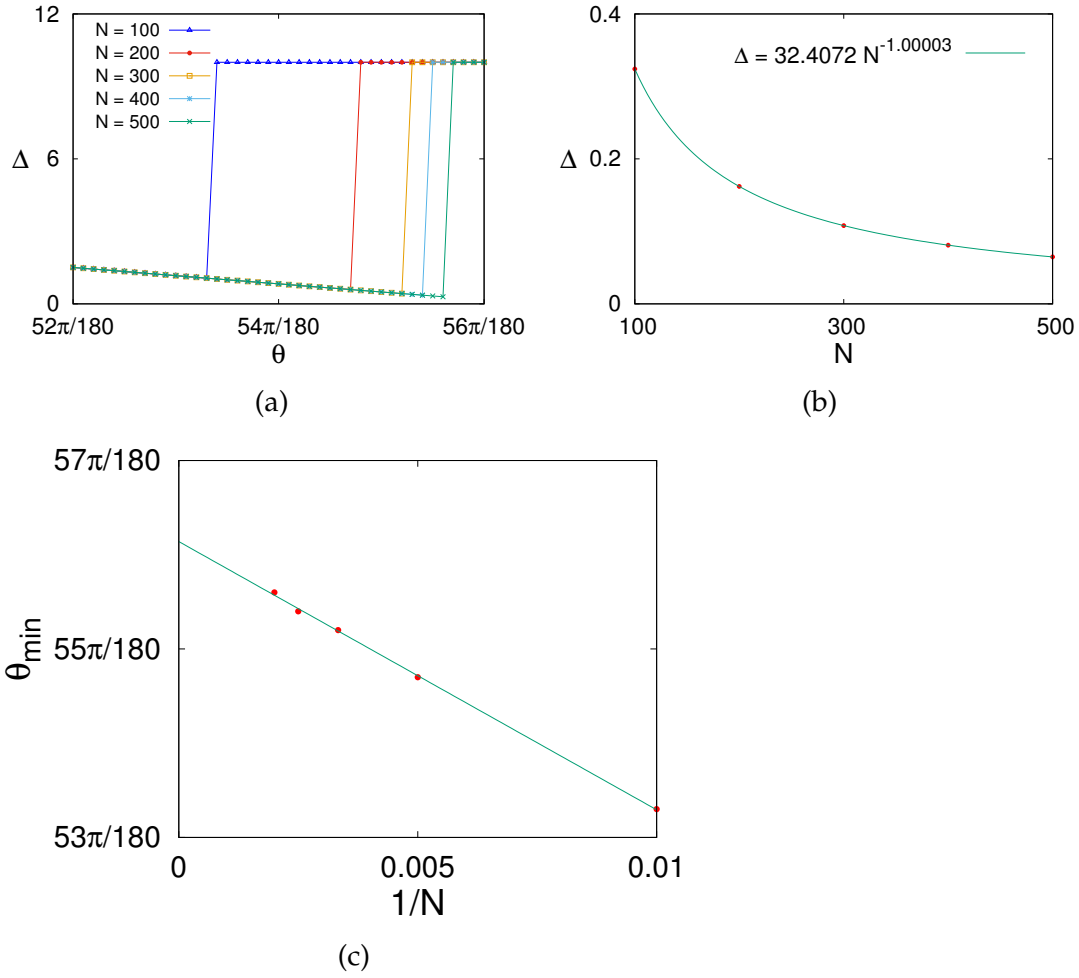


Figure 2.4.21: Finite-size scaling of the energy gap: $\gamma = \pi/6$. (a) The energy gap $\Delta$ is plotted as a function of the polarization angle $\theta$ and different system sizes $N$. From left to right, the energy gap gradually decreases, reaches a minimum and increases significantly when the system undergoes a phase transition. We denote the value of $\theta$ by $\theta_{\text{min}}$ when the gap is minimum. (b) The energy gap is plotted as a function of the system size at $\theta = 0.3167\pi$ which is near the phase transition point. The line of best fit is $\Delta = 32.4072N^{-1.00003}$, which implies that the energy gap scales polynomially with the system size. (c) By plotting $\theta_{\text{min}}$ against $1/N$, we extrapolate the phase transition point in the thermodynamic limit $N \to \infty$ as $\theta = (0.3119 \pm 1.2155 \times 10^{-4})\pi$. Figures also appear in [83].

# Chapter 3

## Randomly-oriented dipoles at unit-filling

### 3.1 Motivation

In the previous project, we studied the quantum phases of plane-polarized dipoles in a zigzag optical lattice at half-filling, taking into account nearest-neighbor (NN) and next-nearest-neighbor (NNN) hopping and interactions. We obtained a complex phase diagram showing the trivial ferromagnetic, antiferromagnetic, dimerized and superfluid phases. Having studied the phases and transitions in that model, we are motivated to consider the same optical lattice but this time with each site containing a dipole that is randomly oriented in a three-dimensional space as shown in Figure 3.1.1. Because a dipole is trapped in each site, there is no hopping and therefore, the system is classical as far as the motion of the center of mass is taken into account. We consider NN and NNN interactions and investigate the minimum energy configurations. If we assign a value to the orientation of a dipole on a given site and call it a degree of freedom, there will be infinitely many degrees of freedom for each dipole in each site. If we consider $N = 100$ lattice sites as before, it becomes a very difficult computational problem. We want to use DMRG to study this

new model. Fortunately, ITensor library [90] has a pre-built module to deal with spin-2 systems. Therefore, we want to map this classical model to a spin-2 model so that each lattice site has five degrees of freedom and perform DMRG calculations. We embark to answer the following questions in this project: At zero temperature, what is the configuration or orientation of these dipoles so that the energy of the system is minimum? How does this configuration depend on the chain opening angle $\gamma$ and the strength of the applied magnetic field $\overrightarrow{B}$? Is the transition between different configurations sharp or smooth? How good is the approximation to the ground state with finite degrees of freedom although, in principle, each lattice site can have infinitely many degrees of freedom?

We will first discuss the classical model where each site has infinitely many degrees of freedom and gain some understanding. Later we will discuss the spin-2 model where each dipole in a site has only five degrees of freedom.

## 3.2 Classical model

Figure 3.1.1 shows an optical lattice in the form of a zigzag chain where each lattice site contains a single molecular dipole, thus preventing double occupancy on each site and the hopping of dipoles between sites. The lattice is on the plane of the paper but the dipoles are randomly oriented in three-dimensional space as shown in Figure 3.2.1 such that the dipole moment vector $\overrightarrow{p}_i$ on a site

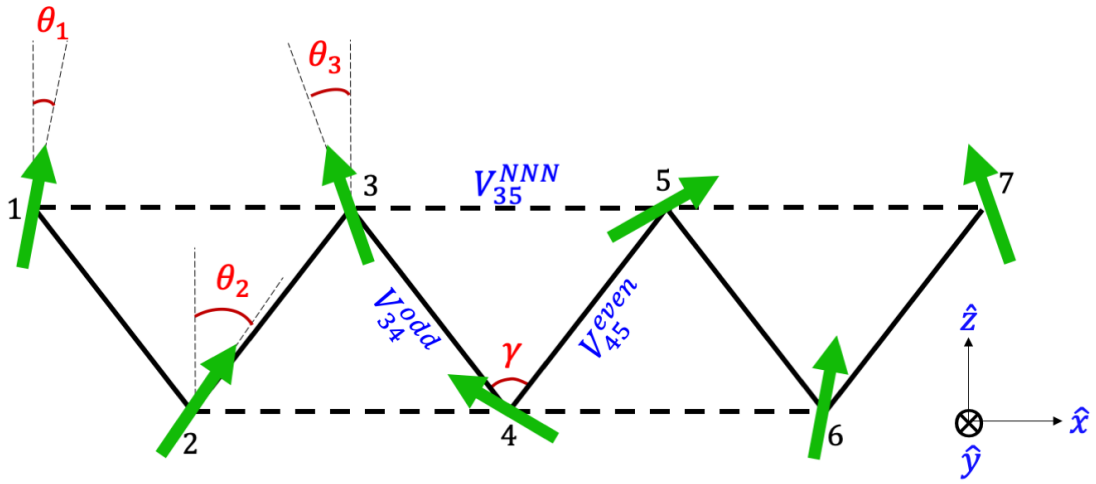


Figure 3.1.1: (Color online) A zigzag chain of dipoles. For our DMRG simulations, we have considered $N = 100$ sites but the figure shows only seven sites labeled 1 through 7. Each site contains a molecular dipole that makes a random angle with the vertical. These are classical dipoles localized in lattice sites - they interact with their nearest (NN) and next-nearest neighbors (NNN) and they do not hop between sites. We label the directions and hence the energy of interactions as odd, even and NNN as shown. Here $\hat{x}$, $\hat{y}$ and $\hat{z}$ are the unit vectors in the positive $x, y$ and $z$ directions respectively such that the zigzag chain lies on the xz plane while the positive y-axis is perpendicular to this plane and is directed into the page.

$i$ is given by

$$\overrightarrow{p}_i = p(\sin\theta_i \cos\phi_i\, \hat{x} + \sin\theta_i \sin\phi_i\, \hat{y} + \cos\theta_i\, \hat{z}). \tag{3.2.1}$$

where $|\overrightarrow{p}_i| = p$ is the magnitude of the $i^{th}$ site dipole moment which is the same for every lattice site, $\theta_i$ is the angle made by the $i^{th}$ site dipole moment with the positive z-axis ($0 \leq \theta_i \leq \pi$), and $\phi_i$ is the angle made by the projection of the $i^{th}$ site dipole moment on the xy-plane with the positive x-axis ($0 \leq \phi_i \leq 2\pi$). We represent the chain opening angle by $\gamma$, and define the unit vectors in the odd, even and NNN directions of the zigzag chain as

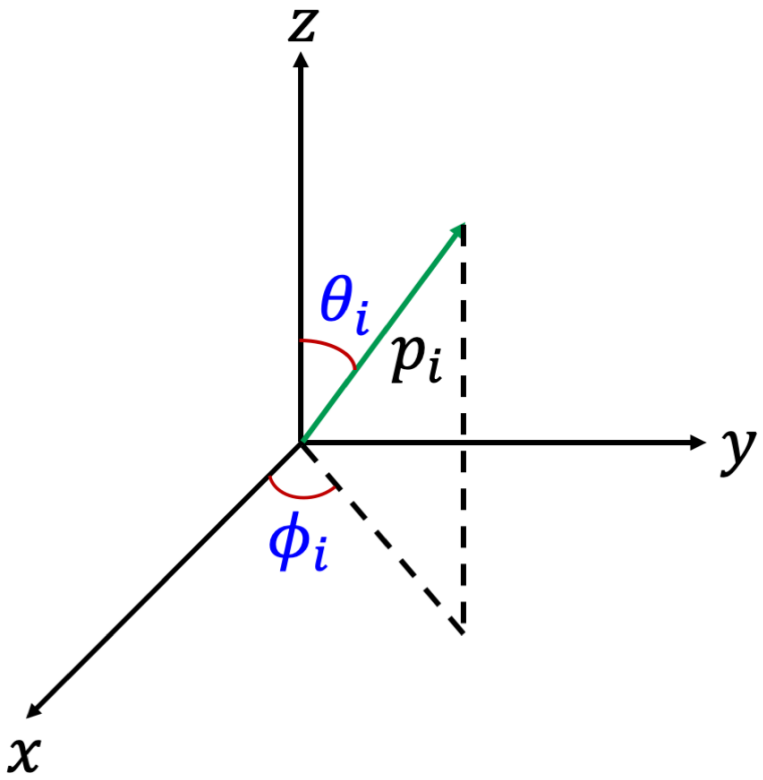


Figure 3.2.1: (Color online) Magnetic moment vector of the dipole at the $i$th site in spherical coordinates $(p_i, \theta_i, \phi_i)$.

$$\begin{aligned} \hat{r}_o &= \sin(\gamma/2)\,\hat{x} - \cos(\gamma/2)\,\hat{z} \\ \hat{r}_e &= \sin(\gamma/2)\,\hat{x} + \cos(\gamma/2)\,\hat{z} \\ \hat{r}_2 &= \hat{x} \end{aligned} \tag{3.2.2}$$

while $r_o, r_e$ and $r_2$ are the lengths of the odd, even and NNN legs of the zigzag chain respectively. Since the distance between two NN sites is the same, we can write $r_o = r_e = r_1$. The distance between two NNN sites is related to that between two NN sites as

$$r_2 = 2r_1 \sin(\gamma/2) \tag{3.2.3}$$

The energy of interaction of a dipole $\overrightarrow{p}_i$ in site $i$ with a magnetic field $\overrightarrow{B}$ is given by

$$V_{i,B} = -\overrightarrow{p}_i.\overrightarrow{B} \tag{3.2.4}$$

while the energy of interaction of dipoles in sites $i$ and $j$ is given by

$$V_{ij} = \frac{1}{4\pi\epsilon_o r_{ij}^3}\Big(\overrightarrow{p}_i.\overrightarrow{p}_j - 3(\overrightarrow{p}_i.\hat{r}_{ij})(\overrightarrow{p}_j.\hat{r}_{ij})\Big) \tag{3.2.5}$$

where $\hat{r}_{ij}$ is one of the three unit vectors $\hat{r}_o, \hat{r}_e$ and $\hat{r}_2$ and $\overrightarrow{r}_{ij}$ is the distance between sites $i$ and $j$. We consider the interaction between nearest and next-nearest neighbors, which means $j = i + 1$ or $i + 2$, and we choose periodic boundary condition. The total energy of a system of $N$ sites is the sum of $V_{i,B}$ and $V_{ij}$ for all $i$ and $j$:

$$
\begin{aligned}
V_{\text{total}} = & \frac{1}{4\pi\epsilon_o r_1^3} \sum_{i=\text{odd}} \left[ \vec{p}_i . \vec{p}_{i+1} - 3(\vec{p}_i . \hat{r}_o)(\vec{p}_{i+1} . \hat{r}_o) \right] \\
& + \frac{1}{4\pi\epsilon_o r_1^3} \sum_{i=\text{even}} \left[ \vec{p}_i . \vec{p}_{i+1} - 3(\vec{p}_i . \hat{r}_e)(\vec{p}_{i+1} . \hat{r}_e) \right] \\
& + \frac{1}{4\pi\epsilon_o r_2^3} \sum_{i=1}^{N} \left[ \vec{p}_i . \vec{p}_{i+2} - 3(\vec{p}_i . \hat{r}_2)(\vec{p}_{i+2} . \hat{r}_2) \right] \\
& - \sum_{i=1}^{N} \vec{p}_i . \vec{B}
\end{aligned} \tag{3.2.6}
$$

Throughout this project we set $p \equiv 1, 4\pi\epsilon_o \equiv 1$ and $r_1 \equiv 1$, and we consider the field in the positive z-direction, i.e., $\vec{B} = B\hat{z}$. Then with some algebra, we can show that

$$
\begin{aligned}
V_{\text{total}} = \sum_i \Bigg[ & \sin\theta_i \sin\theta_{i+1} \cos\phi_i \cos\phi_{i+1} \Big( 1 - 3\sin^2(\gamma/2) \Big) \\
& + \cos\theta_i \cos\theta_{i+1} \Big( 1 - 3\cos^2(\gamma/2) \Big) + \sin\theta_i \sin\theta_{i+1} \sin\phi_i \sin\phi_{i+1} \\
& - \frac{3}{2}(-1)^i \sin\gamma \Big( \cos\theta_i \sin\theta_{i+1} \cos\phi_{i+1} + \sin\theta_i \cos\theta_{i+1} \cos\phi_i \Big) \\
& + \frac{1}{8\sin^3(\gamma/2)} \Big( \sin\theta_i \sin\theta_{i+2} \left( \sin\phi_i \sin\phi_{i+2} - 2\cos\phi_i \cos\phi_{i+2} \right) \\
& \qquad + \cos\theta_i \cos\theta_{i+2} \Big) \\
& - B\cos\theta_i \Bigg]
\end{aligned} \tag{3.2.7}
$$

Equation 3.2.7 implies that for a lattice of $N$ sites, the total energy depends on the values of $2N+2$ different parameters, i.e., $(\gamma, B, \theta_1, \ldots, \theta_N, \phi_1 \ldots \phi_N)$. We set

$N = 100$ and $B = 0$, and embark to find the minimum energy configuration of the system for any given value of $\gamma$. For the energy to be minimum, we assume that

$$\theta_i = \begin{cases} \theta_{\text{odd}}, & \text{if } i = \text{odd} \\ \theta_{\text{even}}, & \text{if } i = \text{even} \end{cases} \tag{3.2.8}$$

and

$$\phi_i = \begin{cases} \phi_{\text{odd}}, & \text{if } i = \text{odd} \\ \phi_{\text{even}}, & \text{if } i = \text{even} \end{cases} \tag{3.2.9}$$

We then plot $V_{\text{total}}$ as a function of $\theta_{\text{odd}}$ and $\theta_{\text{even}}$ for various combinations of $(\phi_{\text{odd}}, \phi_{\text{even}})$ to investigate where the energy is minimum. Figure 3.2.2 shows the values of total energy for the combinations $(\phi_{\text{odd}}, \phi_{\text{even}}) = (0, 0)$ and $(\phi_{\text{odd}}, \phi_{\text{even}}) = (0, \pi)$ when $\gamma = \pi/6$. Although both the plots look qualitatively similar, the lowest possible energy for the former is $-1362.05$ while that for the latter is $-1521.86$ with $\theta_{\text{odd}} = \theta_{\text{even}} = \pi/2$ for either case. This implies that the minimum energy configuration for $\gamma = \pi/6$ in the absence of external magnetic field is the antiferromagnetic phase which means that the dipoles in adjacent lattice sites are point in opposite directions along the x-axis. Similarly, figure 3.2.3 shows the results for $\gamma = \pi$ for the combinations $(\phi_{\text{odd}}, \phi_{\text{even}}) = (0, 0)$ and $(\phi_{\text{odd}}, \phi_{\text{even}}) = (0, \pi)$ where the former gives the lowest possible energy $-225$

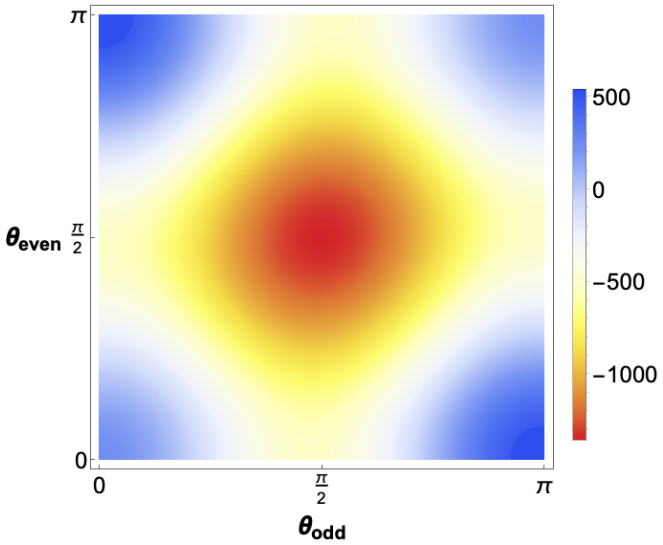


(a) $(\phi_{\text{odd}}, \phi_{\text{even}}) = (0, 0)$

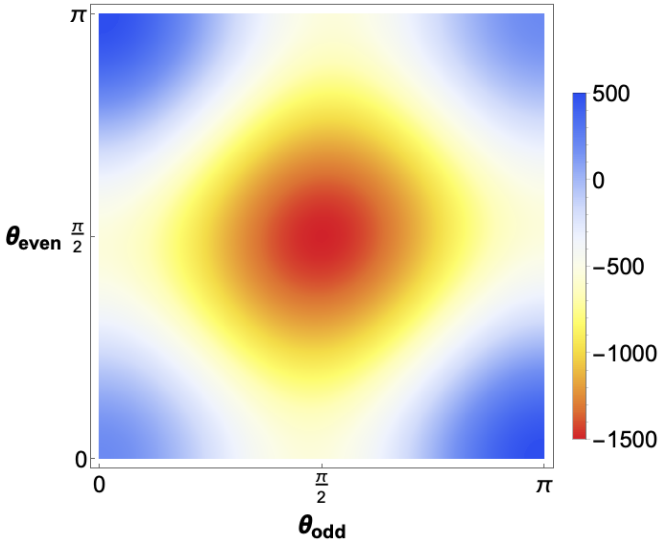


(b) $(\phi_{\text{odd}}, \phi_{\text{even}}) = (0, \pi)$

Figure 3.2.2: $(\gamma, B) = (\pi/6, 0)$: Total energy given by Equation 3.2.7 as a function of the angles $\theta_{\text{odd}}$ and $\theta_{\text{even}}$ for (a) $(\phi_{\text{odd}}, \phi_{\text{odd}}) = (0, 0)$ and (b) $(\phi_{\text{odd}}, \phi_{\text{odd}}) = (0, \pi)$. The energy is minimum, $V_{\text{total, min}} = -1521.86$, when $(\phi_{\text{odd}}, \phi_{\text{odd}}) = (0, \pi)$ and $\theta_{\text{odd}} = \theta_{\text{even}} = \pi/2$, which represents an antiferromagnetic phase meaning the dipoles in adjacent sites are in opposite directions along the x-axis.

when $\theta_{\text{odd}} = \theta_{\text{even}} = \pi/2$. This implies that the minimum energy configuration is ferromagnetic which means all the dipoles point in the same direction (either positive x or negative x). It is interesting to note that for the two cases ($\gamma = \pi/6$)

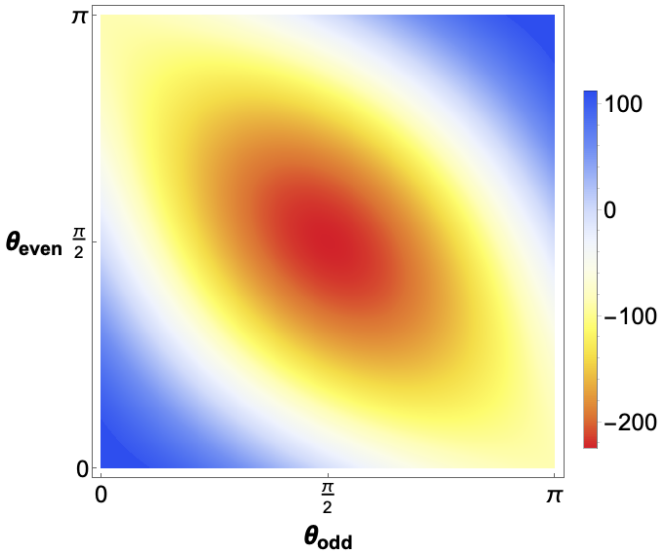


(a) $(\phi_{\text{odd}}, \phi_{\text{even}}) = (0, 0)$

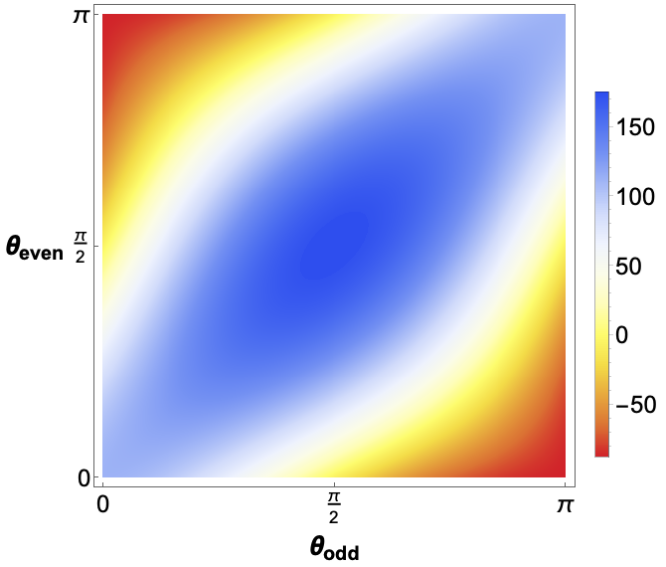


(b) $(\phi_{\text{odd}}, \phi_{\text{even}}) = (0, \pi)$

Figure 3.2.3: $(\gamma, B) = (\pi, 0)$: Total energy given by Equation 3.2.7 as a function of the angles $\theta_{\text{odd}}$ and $\theta_{\text{even}}$ for (a) $(\phi_{\text{odd}}, \phi_{\text{odd}}) = (0, 0)$ and (b) $(\phi_{\text{odd}}, \phi_{\text{odd}}) = (0, \pi)$. The energy is minimum, $V_{\text{total, min}} = -225$, when $(\phi_{\text{odd}}, \phi_{\text{odd}}) = (0, 0)$ and $\theta_{\text{odd}} = \theta_{\text{even}} = \pi/2$, which corresponds to a ferromagnetic phase meaning all the dipoles are oriented in either positive or negative x-direction.

and $\pi$, the minimum energy configurations are such that the dipoles are in the plane of the zigzag optical lattice. Additionally, we carry out several Monte

Carlo simulations to minimize $V_{\text{total}}$ as a function of $\gamma, B, \theta_1, \ldots, \theta_N, \phi_1 \ldots \phi_N$. We never find a minimum energy configuration where the dipoles are oriented out of the plane of the zigzag chain.

## 3.3 Spin-2 model

The magnetic moment of the dipole at site $i$ is proportional to its total spin $\overrightarrow{S}_i = S_i^x\hat{x} + S_i^y\hat{y} + S_i^z\hat{z}$, therefore the dipole moment vector in Equation 3.2.1 can be written as

$$\overrightarrow{p}_i = k\overrightarrow{S}_i \tag{3.3.1}$$

where $k$ is a proportionality constant. We set $k \equiv 1$. Then Equation 3.2.5 for this situation becomes

$$V_{ij} = \frac{1}{r_{ij}^3}\Big(\overrightarrow{S}_i.\overrightarrow{S}_j - 3(\overrightarrow{S}_i.\hat{r}_{ij})(\overrightarrow{S}_j.\hat{r}_{ij})\Big) \tag{3.3.2}$$

The Hamiltonian of the system is the sum of all the interactions in the odd, even and NNN directions plus the energy of interaction of each dipole with the applied field $\overrightarrow{B}$:

$$
\begin{aligned}
H = \sum_j \Bigg[ & S_j^x S_{j+1}^x + S_j^y S_{j+1}^y + S_j^z S_{j+1}^z \\
& - 3\Big(S_j^x S_{j+1}^x sin^2(\gamma/2) + S_j^z S_{j+1}^z cos^2(\gamma/2)\Big)\Bigg] \\
& + \frac{3}{2} sin(\gamma) \sum_{j=\text{odd}} \Big(S_j^x S_{j+1}^z + S_j^z S_{j+1}^x\Big) \\
& - \frac{3}{2} sin(\gamma) \sum_{j=\text{even}} \Big(S_j^x S_{j+1}^z + S_j^z S_{j+1}^x\Big) \\
& + \frac{1}{8\sin^3(\gamma/2)} \sum_j \Big[S_j^x S_{j+2}^x + S_j^y S_{j+2}^y + S_j^z S_{j+2}^z - 3 S_j^x S_{j+2}^x\Big] \\
& - B \sum_j S_j^z
\end{aligned}
\tag{3.3.3}
$$

It should be noted that the Hamiltonian is a function of $\gamma$ and $B$. We choose open boundary condition because we want to use DMRG for this Hamiltonian and DMRG works poorly with periodic boundary condition.

## 3.4 Phase diagram

Figure 3.4.1 shows the ground state phase diagram of the system for different values of chain opening angle $\gamma$ and applied magnetic field $B$. Every DMRG calculation leading to this diagram has been performed targeting different initial states but only the ground state with the lowest possible energy has been considered. We have explained in the previous research project how the initial states affect the final results obatined with DMRG. The phase diagram has been produced using the values of the order parameters for the different phases. The

different phases, and the correlation functions and order parameters used to identify them will be discussed in the subsequent paragraphs.

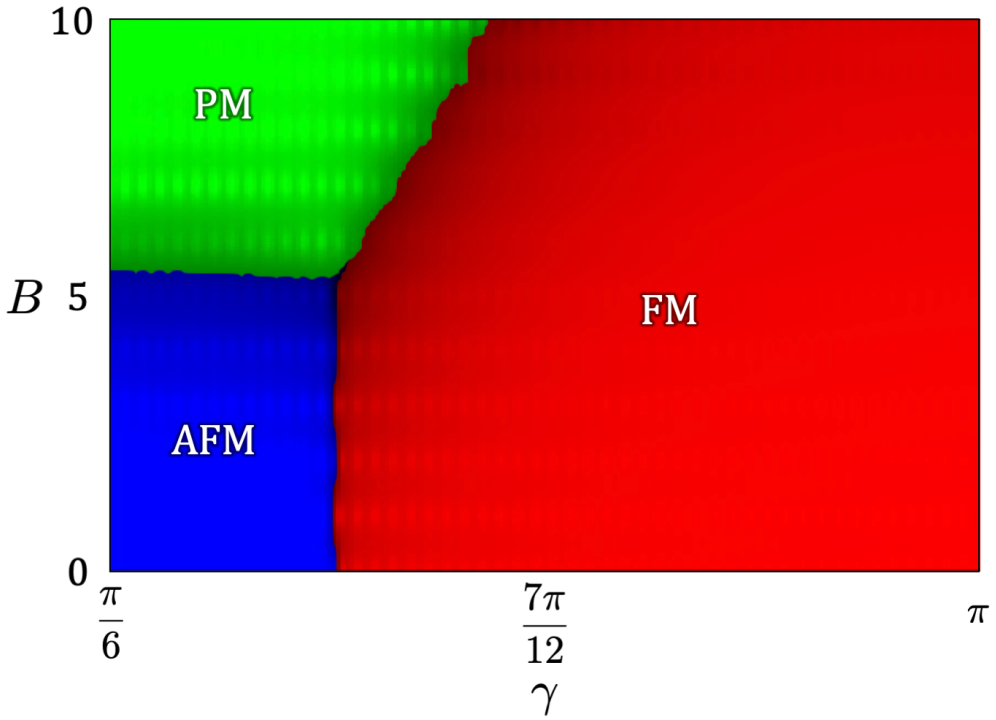


Figure 3.4.1: (Color online) Ground state phase diagram. Each color is associated with a different phase; the brighter a color, the deeper the system in that phase. The system exhibits only three phases: ferromagnetic (FM) that has all the spins pointing in the same direction, antiferromagnetic (AFM) where spins in adjacent lattice sites point in opposite directions, and paramagnetic (PM) where all the spins point in the direction of the applied field. All the phases and their boundaries have been drawn using the values of order parameters for the system size $N = 100$.

### 3.4.1 Ferromagnetic phase

When all the dipoles in the lattice are oriented in the same direction to minimize their energy, we call the phase ferromagnetic (FM). Figure 3.4.2 shows the values of the NN correlation $\langle S_j^x S_{j+1}^x \rangle$ and the long-range correlation $\langle S_1^x S_j^x \rangle$ in the absence of the field, implying that all the dipoles are oriented in either

positive or negative x-direction. This is expected because the lattice is linear ($\gamma = \pi$) in this case, which means the NN interactions are much stronger than the NNN interactions and the only way the energy of the system can be minimized is by having the head of a dipole pointing towards the tail of its nearest neighbor.

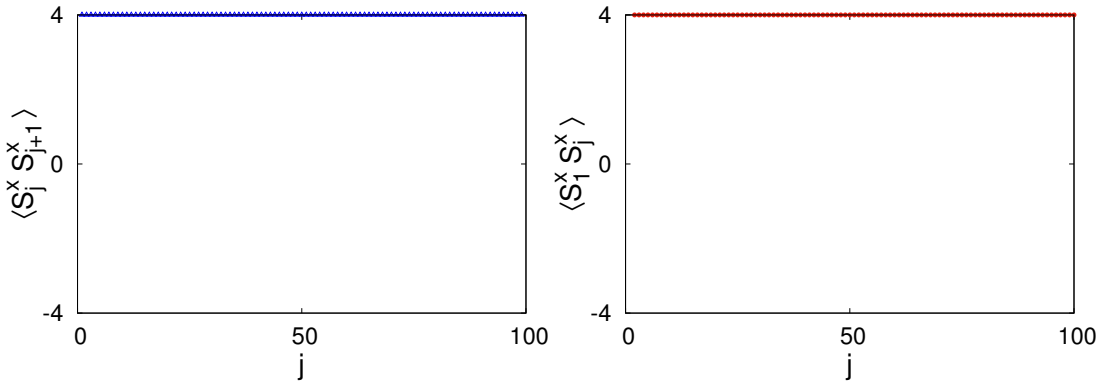


(a) (b)

Figure 3.4.2: (Color online) FM phase. $(\gamma, B) = (\pi, 0)$

### 3.4.2 Antiferromagnetic phase

When the chain opening angle is small, $\gamma < \pi/3$ to be specific, the distance between the NNN dipoles is smaller than that between NN dipoles. In the absence of magnetic field, we expect a pair of NNN dipoles chosen at random to point in the same direction while we also expect a pair of NN dipoles to point in opposite directions. This should result in what we call an antiferromagnetic (AFM) phase and this is exactly what Figure 3.4.3 shows.

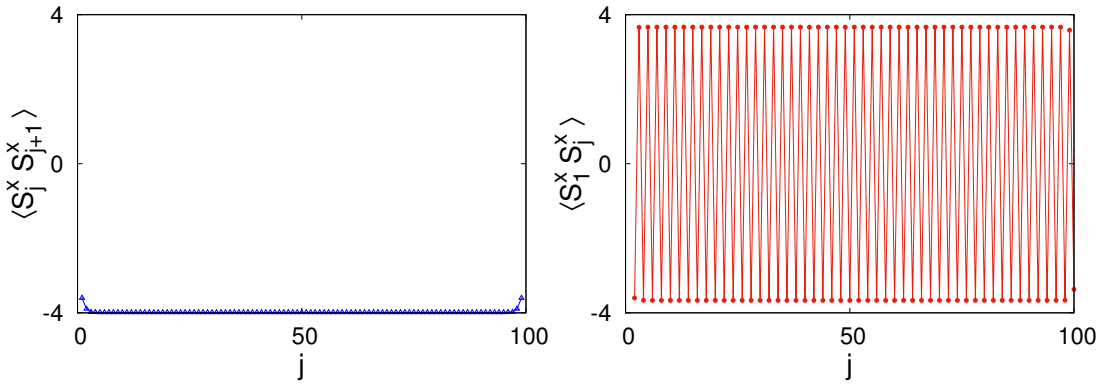


(a) (b)

Figure 3.4.3: (Color online) AFM phase. $(\gamma, B) = (\pi/6, 0)$.

### 3.4.3 Paramagnetic phase

We expect the dipoles to point in the direction of the magnetic field when the field is strong and we call the corresponding phase paramagnetic (PM). For a small chain opening angle $\gamma = \pi/6$ and a field strength $B = 10$, we obtain such a phase as shown in Figure 3.4.4 and this is exactly as expected. It should be noted that the phase diagram (Figure 3.4.1) shows that the linear chain is still in FM phase for this field strength, meaning a much stronger field is needed to drive the system into PM phase.

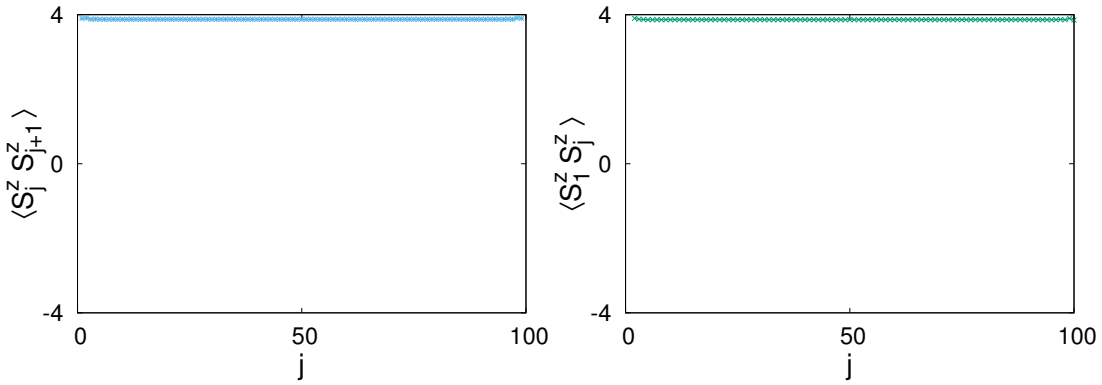


Figure 3.4.4: (Color online) PM phase. $(\gamma, B) = (\pi/6, 10)$.

### 3.4.4 Order parameters and phase transitions

We define the order parameters for ferromagnetic, antiferromagnetic, z-dimer and xy-dimer phases as follows:

$$O_{\text{ferro}} = \frac{4}{N} \sum_{i=\frac{N}{4}+1}^{\frac{N}{2}} \left| \sum_{j=\frac{3N}{4}}^{\frac{3N}{4}+3} \langle S_i^x S_j^x \rangle \right| \tag{3.4.1}$$

$$O_{\text{neel}} = \frac{4}{N} \sum_{i=\frac{N}{4}+1}^{\frac{N}{2}} \left| \sum_{j=\frac{3N}{4}}^{\frac{3N}{4}+3} (-1)^j \langle S_i^x S_j^x \rangle \right| \tag{3.4.2}$$

$$O_{\text{para}} = \frac{4}{N} \sum_{i=\frac{N}{4}+1}^{\frac{N}{2}} \left| \sum_{j=\frac{3N}{4}}^{\frac{3N}{4}+3} \langle S_i^z S_j^z \rangle \right| \tag{3.4.3}$$

As shown in the equations, we minimize the edge effects due to open boundaries by defining the order parameters as average expectation values of the

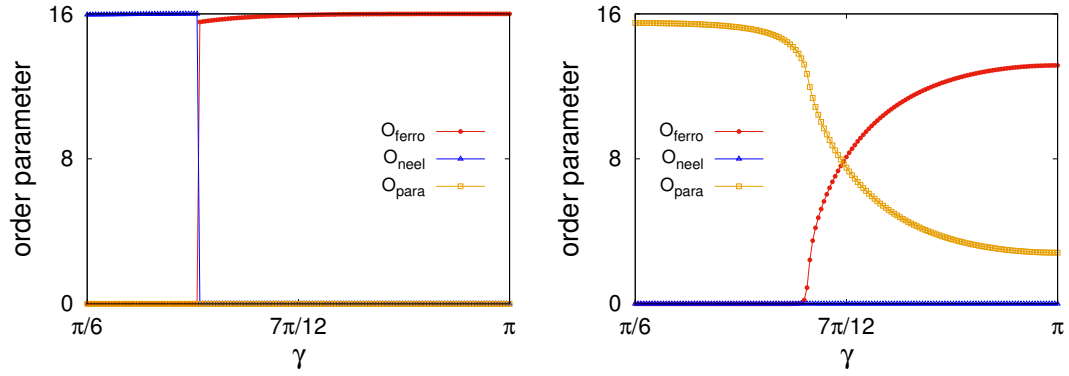


(a) $B = 0$ (b) $B = 10$

Figure 3.4.5: Order parameter for various phases as a function of chain opening angle $\gamma$

correlators between dipoles in the middle part of the chain, a method similar to one in the paper by Rossini et. al. [99].

As mentioned earlier, the phase diagram has been produced using the values of the order parameters. The way we have defined these parameters, their values range between 0 and 16 for all the phases. Figure 3.4.5a shows that the transition between AFM and FM phases is sharp in the absence of field. Similarly, Figure 3.4.5b depicts the situation in the presence of a strong field $B = 10$, where we see a smooth transition between the FM and PM phases.

# Chapter 4

## Summary and conclusion

In our first project, we have numerically studied the ground-state properties of dipoles polarized at an angle in the plane of the zigzag optical lattice by taking into account hopping and interactions up to second neighbors. Even though this is a rather simple model, it comprises of frustrated regimes that lead to a rich phase diagram. We have used a novel approach to write the Hamiltonian that gives an intuitive understanding of the model, makes it convenient to identify frustrated and non-frustrated regimes, and helps predict the ground states beforehand so that the results obtained from numerical simulations can be verified. We have observed all the phases that Wang et. al. [71] obtained. Nevertheless, in contrast to what was shown in their phase diagrams, we have observed a sharp transition between FM and AFM phases. We are, however, unable to find any spin liquid, Haldane or topological phase in this system.

Similarly, in our second project, we have studied a classical model of dipoles randomly oriented in a zigzag optical lattice. After exploring the model classically and predicting minimum energy configurations for some special cases, we have used a spin-2 model to investigate the system using DMRG. The results obtained from DMRG show that the minimum energy configurations are

such that the dipoles are always in the plane of the zigzag chain. We have produced a phase diagram for a lattice of $N = 100$ sites that consists of three phases: ferromagnetic (FM), antiferromagnetic (AFM) and paramagnetic (PM). We have observed a sharp transition between FM and AFM phases for a small chain opening angle in the absence of the field and a smooth transition between FM and PM phases for a linear lattice in the presence of a strong field. We have not obtained the phase boundaries in the thermodynamic limit $N \to \infty$ and this is work in progress. There are still some open questions and we expect to answer them in the future. The questions are: Why are the dipoles always in the plane of the zigzag chain for the energy to be minimum? How good an approximation is a spin-2 model where each lattice site has only five degrees of freedom to a classical model where each site can have infinite degrees of freedom? If it is a good approximation, is there any frustrated regime in the spin-2 version and if there is, would that lead to any interesting quantum effects?

# Appendix A

## DMRG code: Plane-polarized dipoles at half-filling

```
#include "itensor/all.h"

using namespace itensor;
using namespace std;

int main(int argc, char* argv[])
    {
    double pi = M_PI;

    //Specify number of lattice sites
    int N = 100;

    //Chain opening angle gamma (in degrees)
   double gamma = 30;
```

```
//c = d_1/lambda where d_1 is the distance between nearest
   neighbors and lambda is a function of lattice depth
double c = 0.1;

//Strength of external magnetic field is zero (it can have
   any arbitrary value, DMRG results will still be the same)
double h = 0;

//The factor -0.5 that appears in front of the (S^+ S^- +
   h.c.) terms in the Hamiltonian
double J_factor = -0.5;

//B_o = 2 J_1 is the relative hopping strength in the odd
   direction
double B_o = 1;

//B_e = 2 J_1 is the relative hopping strength in the even
   direction
double B_e = B_o;

//B_e = 2 J_2 is the relative hopping strength in the
```

```
   next-nearest-neighbor (NNN) direction
double B_2 = B_o * exp(-c*(2 * sin ((gamma*pi/180)/2) - 1) );


//Create a one-dimensional array of N rows to store the
   initial state
int v[N]={};


//Make Neel state the initial state
for(int i = 0; i < N; i++)
  {
  if(i%2 == 0)
    {
    v[i] = 0;
    }
  else
    {
    v[i] = 1;
    }
  }


 //Polarization angle theta (in degrees)
```

```
double theta = 90;


//Write equations for dipole-dipole interaction strengths in
   the even, odd and NNN directions
double V1even = 1 - 3 * pow(cos(pi - (gamma*pi/180)/2 -
   theta*pi/180), 2);


double V1odd = 1 - 3 * pow(cos((gamma*pi/180)/2 -
   theta*pi/180), 2);


double V2 = (1/pow((2*(1 - cos(gamma*pi/180))), 1.5)) * (1 -
   3 * pow(cos(pi/2 - theta*pi/180), 2));


//Write the equations for "relative" interaction strengths in
   the three directions
double a_o = V1odd/B_o;


double a_e = V1even/B_e;


double a_2 = V2/B_2;
```

```
//Initialize the site degrees of freedom.
auto sites = SpinHalf(N); //Make a chain of N spin 1/2's


auto ampo = AutoMPO(sites);


for(int j = 1; j < N; ++j)
  {
    if(j%2 != 0)
      {
      ampo += B_o * J_factor,"S+",j,"S-",j+1;
    ampo += B_o * J_factor,"S-",j,"S+",j+1;
      ampo += B_o * a_o,"Sz",j,"Sz",j+1;
      }
    else
      {
      ampo += B_e * J_factor,"S+",j,"S-",j+1;
    ampo += B_e * J_factor,"S-",j,"S+",j+1;
      ampo += B_e * a_e,"Sz",j,"Sz",j+1;
      }
  }
```

```
for(int j = 1; j < N-1; ++j)
      {
      ampo += B_2 * J_factor,"S+",j,"S-",j+2;
      ampo += B_2 * J_factor,"S-",j,"S+",j+2;

      ampo += B_2 * a_2,"Sz",j,"Sz",j+2;
      }

for(int j = 1; j <= N; ++j)
      {
      ampo += h,"Sz",j;
      }

 //Hamiltonian conserving the total quantum number
auto H = IQMPO(ampo);

auto initState = InitState(sites);

cout << "\nInitial wavefunction MPS mapped to vector v(N):
   \n";
```

```
for(int i = 1; i <= N; ++i)
      {
      if(v[i] == 1)
         {
         initState.set(i,"Up"); //Up means spin up
      cout << "1 ";
      }
      else
         {
         initState.set(i,"Dn"); //Dn mean spin down
      cout << "0 ";
      }
      }

 //Initial matrix product state conserving the total quantum
    number
auto psi = IQMPS(initState);

printfln("\n\nInitial energy = %.5f", overlap(psi,H,psi) );

//Specify the accuracy parameters such as number of sweeps,
```

```
   maximum numbers of states kept in each sweep, etc.
auto sweeps = Sweeps(7);
sweeps.maxm() = 10,20,80,200,300,400,400;
sweeps.minm() = 1,1,1,1,1,1,1;
sweeps.cutoff() = 1E-5,1E-6,1E-7,1E-8,1E-8,1E-8;
sweeps.niter() = 4,3,3,2,2,2,2;
sweeps.noise() = 1E-5,1E-5,1E-8,1E-9,1E-10,1E-10,1E-10;
println(sweeps);


//Begin the DMRG calculation
auto energy = dmrg(psi,H,sweeps,{"Quiet=",true});


//Print the final energy reported by DMRG
printfln("\nGround State Energy = %.10f",energy);
printfln("\nUsing overlap = %.10f", overlap(psi,H,psi) );
println("\nTotal QN of Ground State = ",totalQN(psi));


cout << "\nd_1/lambda = " << c << endl;
cout << "\nN = " << N << ", gamma = " << gamma << ", theta =
   " << theta << endl;
cout << "\nB_o = " << B_o << ", B_e = " << B_e << ", B_2 = "
```

```
   << B_2 << endl;
cout << "\na_o = " << a_o << ", " << "a_e = " << a_e << ", "
   << "a_2 = " << a_2 << endl;

println("\n\n#j \t <S^z_j>");

for(int j=1; j <= N; ++j)
  {
  //re-gauge psi to get ready to measure at position j
  psi.position(j);

  ITensor ket = psi.A(j);
  ITensor bra = dag(prime(ket,Site));

  ITensor Szjop = sites.op("Sz",j);

  //take an inner product
  auto szj = (bra*Szjop*ket).real();

  printfln("%d \t %.12f",j,szj);
  }
```

```
println("\n\n#j \t <Sˆz_j Sˆz_{j+1}>");


for(int i = 1; i < N; ++i)
  {
  int j = i+1;


  auto Sz_i = sites.op("Sz",i);
  auto Sz_j = sites.op("Sz",j);


  //'Gauge' the MPS to site i (Any 'position' between i and
     j, inclusive, would work here)
  psi.position(i);


  //index linking i to i+1:
  auto ir = commonIndex(psi.A(i),psi.A(i+1),Link);


  auto C = psi.A(i)*Sz_i*dag(prime(psi.A(i),Site,ir));
  for(int k = i+1; k < j; ++k)
    {
    C *= psi.A(k);
```

```
    C *= dag(prime(psi.A(k),Link));

    }

  C *= psi.A(j);

  C *= Sz_j;


  //Index linking j to j-1:

  auto jl = commonIndex(psi.A(j),psi.A(j-1),Link);

  C *= dag(prime(psi.A(j),jl,Site));


  printfln("%d \t %.12f",i,C.real());

  }


println("\n\n#j \t <S^+_j S^-_{j+1}>");


for(int i = 1; i < N; ++i)

  {

  int j = i+1;


  auto Sp_i = sites.op("S+",i);

  auto Sm_j = sites.op("S-",j);
```

```
    psi.position(i);

    auto ir = commonIndex(psi.A(i),psi.A(i+1),Link);

    auto C = psi.A(i)*Sp_i*dag(prime(psi.A(i),Site,ir));
    for(int k = i+1; k < j; ++k)
      {
      C *= psi.A(k);
      C *= dag(prime(psi.A(k),Link));
      }
    C *= psi.A(j);
    C *= Sm_j;

    auto jl = commonIndex(psi.A(j),psi.A(j-1),Link);
    C *= dag(prime(psi.A(j),jl,Site));

    printfln("%d \t %.12f",i,C.real());
    }

  int l = 1;
```

```
println("\n\n#j \t <S^z_1 S^z_j>");


for(int j = l+1; j <= N; ++j)
  {
  auto Sz_l = sites.op("Sz",l);
  auto Sz_j = sites.op("Sz",j);


  psi.position(l);


  auto lr = commonIndex(psi.A(l),psi.A(l+1),Link);


  auto C = psi.A(l)*Sz_l*dag(prime(psi.A(l),Site,lr));
  for(int k = l+1; k < j; ++k)
    {
    C *= psi.A(k);
    C *= dag(prime(psi.A(k),Link));
    }
  C *= psi.A(j);
  C *= Sz_j;


  auto jl = commonIndex(psi.A(j),psi.A(j-1),Link);
```

```
  C *= dag(prime(psi.A(j),jl,Site));

  printfln("%d \t %.12f",j,C.real());
  }

println("\n\n#j \t <S^+_1 S^-_j>");

for(int j = l+1; j <= N; ++j)
  {
  auto Sp_l = sites.op("S+",l);
  auto Sm_j = sites.op("S-",j);

  psi.position(l);

  auto lr = commonIndex(psi.A(l),psi.A(l+1),Link);

  auto C = psi.A(l)*Sp_l*dag(prime(psi.A(l),Site,lr));
  for(int k = l+1; k < j; ++k)
    {
    C *= psi.A(k);
    C *= dag(prime(psi.A(k),Link));
```

```
    }
  C *= psi.A(j);
  C *= Sm_j;

  auto jl = commonIndex(psi.A(j),psi.A(j-1),Link);
  C *= dag(prime(psi.A(j),jl,Site));

  printfln("%d \t %.12f",j,C.real());
  }

return 0;
}
```

# Bibliography


[1] Christian Gross and Immanuel Bloch. Quantum simulations with ultracold atoms in optical lattices. *Science*, 357(6355):995–1001, 2017.

[2] I. M. Georgescu, S. Ashhab, and Franco Nori. Quantum simulation. *Rev. Mod. Phys.*, 86:153–185, 2014.

[3] Rudolf Grimm, Matthias Weidemller, and Yurii B. Ovchinnikov. Optical dipole traps for neutral atoms. volume 42 of *Advances In Atomic, Molecular, and Optical Physics*, pages 95 – 170. Academic Press, 2000.

[4] N. Goldman, J. C. Budich, and P. Zoller. Topological quantum matter with ultracold gases in optical lattices. *Nature Physics*, 12:639, 2016.

[5] Andrew J. Daley. Viewpoint: Towards an atomtronic diode. *Physics*, 2015.

[6] T. Langen, R. Geiger, M. Kuhnert, B. Rauer, and J. Schmiedmayer. Local emergence of thermal correlations in an isolated quantum many-body system. *Nature Physics*, 9:640, 2013.

[7] Tim Langen, Sebastian Erne, Remi Geiger, Bernhard Rauer, Thomas Schweigler, Maximilian Kuhnert, Wolfgang Rohringer, Igor E. Mazets, Thomas Gasenzer, and Jörg Schmiedmayer. Experimental observation of a generalized gibbs ensemble. *Science*, 348(6231):207–211, 2015.

[8] Adam M. Kaufman, M. Eric Tai, Alexander Lukin, Matthew Rispoli, Robert Schittko, Philipp M. Preiss, and Markus Greiner. Quantum thermalization through entanglement in an isolated many-body system. *Science*, 353(6301):794–800, 2016.

[9] Rahul Nandkishore and David A. Huse. Many-body localization and thermalization in quantum statistical mechanics. *Annual Review of Condensed Matter Physics*, 6(1):15–38, 2015.

[10] Ehud Altman and Ronen Vosk. Universal dynamics and renormalization in many-body-localized systems. *Annual Review of Condensed Matter Physics*, 6(1):383–409, 2015.

[11] Immanuel Bloch. Ultracold quantum gases in optical lattices. *Nature Physics*, 1(1):23–30, 2005.

[12] Matthew P. A. Fisher, Peter B. Weichman, G. Grinstein, and Daniel S. Fisher. Boson localization and the superfluid-insulator transition. *Phys. Rev. B*, 40:546–570, 1989.

[13] D. Jaksch, C. Bruder, J. I. Cirac, C. W. Gardiner, and P. Zoller. Cold bosonic atoms in optical lattices. *Phys. Rev. Lett.*, 81:3108–3111, 1998.

[14] Markus Greiner, Olaf Mandel, Tilman Esslinger, Theodor W. Hänsch, and Immanuel Bloch. Quantum phase transition from a superfluid to a mott insulator in a gas of ultracold atoms. *Nature*, 415(6867):39–44, 2002.

[15] C. Orzel, A. K. Tuchman, M. L. Fenselau, M. Yasuda, and M. A. Kasevich. Squeezed states in a bose-einstein condensate. *Science*, 291(5512):2386–2389, 2001.

[16] M. Girardeau. Relationship between systems of impenetrable bosons and fermions in one dimension. *Journal of Mathematical Physics*, 1(6):516–523, 1960.

[17] Belén Paredes, Artur Widera, Valentin Murg, Olaf Mandel, Simon Fölling, Ignacio Cirac, Gora V. Shlyapnikov, Theodor W. Hänsch, and Immanuel Bloch. Tonks-girardeau gas of ultracold atoms in an optical lattice. *Nature*, 429(6989):277–281, 2004.

[18] Toshiya Kinoshita, Trevor Wenger, and David S. Weiss. Observation of a one-dimensional tonks-girardeau gas. *Science*, 305(5687):1125–1128, 2004.

[19] B. DeMarco and D. S. Jin. Onset of fermi degeneracy in a trapped atomic gas. *Science*, 285(5434):1703–1706, 1999.

[20] Andrew G. Truscott, Kevin E. Strecker, William I. McAlexander, Guthrie B. Partridge, and Randall G. Hulet. Observation of fermi pressure in a gas of trapped atoms. *Science*, 291(5513):2570–2572, 2001.

[21] C. A. Regal, M. Greiner, and D. S. Jin. Observation of resonance condensation of fermionic atom pairs. *Phys. Rev. Lett.*, 92:040403, 2004.

[22] C. Chin, M. Bartenstein, A. Altmeyer, S. Riedl, S. Jochim, J. Hecker Denschlag, and R. Grimm. Observation of the pairing gap in a strongly interacting fermi gas. *Science*, 305(5687):1128–1130, 2004.

[23] M. W. Zwierlein, J. R. Abo-Shaeer, A. Schirotzek, C. H. Schunck, and W. Ketterle. Vortices and superfluidity in a strongly interacting fermi gas. *Nature*, 435(7045):1047–1051, 2005.

[24] Immanuel Bloch. Quantum gases in optical lattices. *Physics World*, 17(4):25–29, 2004.

[25] Tilman Esslinger. Fermi-hubbard physics with atoms in an optical lattice. *Annual Review of Condensed Matter Physics*, 1(1):129–152, 2010.

[26] W. Hofstetter, J. I. Cirac, P. Zoller, E. Demler, and M. D. Lukin. High-temperature superfluidity of fermionic atoms in optical lattices. *Phys. Rev. Lett.*, 89:220407, 2002.

[27] Patrick A. Lee, Naoto Nagaosa, and Xiao-Gang Wen. Doping a mott insulator: Physics of high-temperature superconductivity. *Rev. Mod. Phys.*, 78:17–85, 2006.

[28] Karyn Le Hur and T. Maurice Rice. Superconductivity close to the mott state: From condensed-matter systems to superfluidity in optical lattices. *Annals of Physics*, 324(7):1452 – 1515, 2009. July 2009 Special Issue.

[29] Cheng Chin, Rudolf Grimm, Paul Julienne, and Eite Tiesinga. Feshbach resonances in ultracold gases. *Rev. Mod. Phys.*, 82:1225–1286, 2010.

[30] T Lahaye, C Menotti, L Santos, M Lewenstein, and T Pfau. The physics of dipolar bosonic quantum gases. *Reports on Progress in Physics*, 72(12):126401, 2009.

[31] M. A. Baranov, M. Dalmonte, G. Pupillo, and P. Zoller. Condensed matter theory of dipolar quantum gases. *Chemical Reviews*, 112(9):5012–5061, 2012.

[32] Kaden R. A. Hazzard, Mauritz van den Worm, Michael Foss-Feig, Salvatore R. Manmana, Emanuele G. Dalla Torre, Tilman Pfau, Michael Kastner, and Ana Maria Rey. Quantum correlations and entanglement in far-from-equilibrium spin systems. *Phys. Rev. A*, 90:063622, 2014.

[33] Axel Griesmaier, Jörg Werner, Sven Hensler, Jürgen Stuhler, and Tilman Pfau. Bose-einstein condensation of chromium. *Phys. Rev. Lett.*, 94:160401, 2005.

[34] Mingwu Lu, Nathaniel Q. Burdick, Seo Ho Youn, and Benjamin L. Lev. Strongly dipolar bose-einstein condensate of dysprosium. *Phys. Rev. Lett.*, 107:190401, 2011.

[35] K. Aikawa, A. Frisch, M. Mark, S. Baier, A. Rietzler, R. Grimm, and F. Ferlaino. Bose-einstein condensation of erbium. *Phys. Rev. Lett.*, 108:210401, 2012.

[36] K.-K. Ni, S. Ospelkaus, M. H. G. de Miranda, A. Pe'er, B. Neyenhuis, J. J. Zirbel, S. Kotochigova, P. S. Julienne, D. S. Jin, and J. Ye. A high phase-space-density gas of polar molecules. *Science*, 322(5899):231–235, 2008.

[37] Johann G. Danzl, Elmar Haller, Mattias Gustavsson, Manfred J. Mark, Russell Hart, Nadia Bouloufa, Olivier Dulieu, Helmut Ritsch, and Hanns-Christoph Nägerl. Quantum gas of deeply bound ground state molecules. *Science*, 321(5892):1062–1066, 2008.

[38] J. Deiglmayr, A. Grochola, M. Repp, K. Mörtlbauer, C. Glück, J. Lange, O. Dulieu, R. Wester, and M. Weidemüller. Formation of ultracold polar molecules in the rovibrational ground state. *Phys. Rev. Lett.*, 101:133004, 2008.

[39] M. Saffman, T. G. Walker, and K. Mølmer. Quantum information with rydberg atoms. *Rev. Mod. Phys.*, 82:2313–2363, 2010.

[40] Y. Manin. *Computable and Uncomputable*. (Sovetskoye Radio Press, Moscow) (in Russian), 1980.

[41] Richard P. Feynman. Simulating physics with computers. *International Journal of Theoretical Physics*, 21(6):467–488, 1982.

[42] M.E. Nielsen, M.A. Nielsen, and I.L. Chuang. *Quantum Computation and Quantum Information*. Cambridge Series on Information and the Natural Sciences. Cambridge University Press, 2000.

[43] W.P. Schleich and H. Walther. *Elements of Quantum Information*. Wiley, 2007.

[44] J. Stolze and D. Suter. *Quantum Computing: A Short Course from Theory to Experiment*. Wiley, 2008.

[45] D. Leibfried, B. DeMarco, V. Meyer, M. Rowe, A. Ben-Kish, J. Britton, W. M. Itano, B. Jelenković, C. Langer, T. Rosenband, and D. J. Wineland. Trapped-ion quantum simulator: Experimental application to nonlinear interferometers. *Phys. Rev. Lett.*, 89:247901, 2002.

[46] A. Friedenauer, H. Schmitz, J. T. Glueckert, D. Porras, and T. Schaetz. Simulating a quantum magnet with trapped ions. *Nature Physics*, 4:757, 2008.

[47] Matthew Neeley, Markus Ansmann, Radoslaw C. Bialczak, Max Hofheinz, Erik Lucero, Aaron D. O'Connell, Daniel Sank, Haohua Wang, James Wenner, Andrew N. Cleland, Michael R. Geller, and John M. Martinis.

Emulation of a quantum spin with a superconducting phase qudit. *Science*, 325(5941):722–725, 2009.

[48] R. Gerritsma, G. Kirchmair, F. Zähringer, E. Solano, R. Blatt, and C. F. Roos. Quantum simulation of the dirac equation. *Nature*, 463:68, 2010.

[49] K. Kim, M.-S. Chang, S. Korenblit, R. Islam, E. E. Edwards, J. K. Freericks, G.-D. Lin, L.-M. Duan, and C. Monroe. Quantum simulation of frustrated ising spins with trapped ions. *Nature*, 465:590, 2010.

[50] B. P. Lanyon, J. D. Whitfield, G. G. Gillett, M. E. Goggin, M. P. Almeida, I. Kassal, J. D. Biamonte, M. Mohseni, B. J. Powell, M. Barbieri, A. Aspuru-Guzik, and A. G. White. Towards quantum chemistry on a quantum computer. *Nature Chemistry*, 2:106, 2010.

[51] Roderich Moessner and Arthur P. Ramirez. Geometrical frustration. *Physics Today*, 59:4, 2006.

[52] Leon Balents. Spin liquids in frustrated magnets. *Nature*, 464:199–208, 2010.

[53] Hung-the Diep. *Frustrated Spin Systems*. World Scientific Publishing Company, 2005.

[54] R. Liebmann. *Lecture Notes in Physics: Statistical Mechanics of Periodic Frustrated Ising Systems*. Springer-Verlag, Berlin, 1986.

[55] G. Toulouse. *Communications on Physics*, 2:115–119, 1977.

[56] J Villain. Spin glass with non-random interactions. *Journal of Physics C: Solid State Physics*, 10(10):1717–1734, 1977.

[57] P.W. Anderson. Resonating valence bonds: A new kind of insulator? *Materials Research Bulletin*, 8(2):153 – 160, 1973.

[58] P. W. ANDERSON. The resonating valence bond state in la2cuo4 and superconductivity. *Science*, 235(4793):1196–1198, 1987.

[59] Subir Sachdev and Kwon Park. Ground states of quantum antiferromagnets in two dimensions. *Annals of Physics*, 298(1):58 – 122, 2002.

[60] Subir Sachdev. Understanding correlated electron systems by a classification of mott insulators. *Annals of Physics*, 303(1):226 – 246, 2003.

[61] N. D. Mermin and H. Wagner. Absence of ferromagnetism or antiferromagnetism in one- or two-dimensional isotropic heisenberg models. *Phys. Rev. Lett.*, 17:1307–1307, 1966.

[62] A.A. Belavin, A.M. Polyakov, and A.B. Zamolodchikov. Infinite conformal symmetry in two-dimensional quantum field theory. *Nuclear Physics B*, 241(2):333 – 380, 1984.

[63] P. Francesco, P. Mathieu, and D. Senechal. *Conformal Field Theory*. Graduate Texts in Contemporary Physics. Springer New York, 2012.

[64] A. Luther and I. Peschel. Single-particle states, kohn anomaly, and pairing fluctuations in one dimension. *Phys. Rev. B*, 9:2911–2919, 1974.

[65] Sidney Coleman. Quantum sine-gordon equation as the massive thirring model. *Phys. Rev. D*, 11:2088–2097, 1975.

[66] A.O. Gogolin, A.A. Nersesyan, and A.M. Tsvelik. *Bosonization and Strongly Correlated Systems*. Cambridge University Press, 2004.

[67] Steven R. White. Density matrix formulation for quantum renormalization groups. *Phys. Rev. Lett.*, 69:2863–2866, 1992.

[68] Steven R. White. Density-matrix algorithms for quantum renormalization groups. *Phys. Rev. B*, 48:10345–10356, 1993.

[69] Romn Ors. A practical introduction to tensor networks: Matrix product states and projected entangled pair states. *Annals of Physics*, 349:117 – 158, 2014.

[70] Ulrich Schollwöck. The density-matrix renormalization group. *Rev. Mod. Phys.*, 77:259–315, 2005.

[71] Qingyang Wang, Johannes Otterbach, and Susanne F. Yelin. Interacting in-plane molecular dipoles in a zigzag chain. *Phys. Rev. A*, 96:043615, 2017.

[72] Finn Lasse Buessen, Max Hering, Johannes Reuther, and Simon Trebst. Quantum spin liquids in frustrated spin-1 diamond antiferromagnets. *Phys. Rev. Lett.*, 120:057201, 2018.

[73] Simeng Yan, David A. Huse, and Steven R. White. Spin-liquid ground state of the s = 1/2 kagome heisenberg antiferromagnet. *Science*, 332(6034): 1173–1176, 2011.

[74] Shunsuke Furukawa, Masahiro Sato, Shigeki Onoda, and Akira Furusaki. Ground-state phase diagram of a spin-$\frac{1}{2}$ frustrated ferromagnetic xxz chain: Haldane dimer phase and gapped/gapless chiral phases. *Phys. Rev. B*, 86:094417, 2012.

[75] S. Greschner, L. Santos, and T. Vekua. Ultracold bosons in zig-zag optical lattices. *Phys. Rev. A*, 87:033609, 2013.

[76] M. Azuma, Z. Hiroi, M. Takano, K. Ishida, and Y. Kitaoka. Observation of a spin gap in srcu$_2$ o$_3$ comprising spin- quasi-1d two-leg ladders. *Phys. Rev. Lett.*, 73:3463–3466, 1994.

[77] A. Läuchli, G. Schmid, and M. Troyer. Phase diagram of a spin ladder with cyclic four-spin exchange. *Phys. Rev. B*, 67:100409, 2003.

[78] Takashi Tonegawa, Kiyomi Okamoto, Toshiya Hikihara, and Tru Sakai. Frustrated s = 1/2 two-leg ladder with different leg interactions. *Journal of Physics: Conference Series*, 828(1):012003, 2017.

[79] Geetanjali Giri, Dayasindhu Dey, Manoranjan Kumar, S. Ramasesha, and Zoltán G. Soos. Quantum phases of frustrated two-leg spin-$\frac{1}{2}$ ladders with skewed rungs. *Phys. Rev. B*, 95:224408, 2017.

[80] Stefan Wessel, B. Normand, Frdric Mila, and Andreas Honecker. Efficient Quantum Monte Carlo simulations of highly frustrated magnets: the frustrated spin-1/2 ladder. *SciPost Phys.*, 3:005, 2017.

[81] Karen A. Hallberg. New trends in density matrix renormalization. *Advances in Physics*, 55(5-6):477–526, 2006.

[82] Ulrich Schollwöck. The density-matrix renormalization group in the age of matrix product states. *Annals of Physics*, 326(1):96 – 192, 2011.

[83] Niraj R. Ghimire and Susanne F. Yelin. Frustrated plane-polarized dipoles in one dimension. Manuscript submitted for publication, arXiv:1810.00646, 2018.

[84] Piotr S. Żuchowski and Jeremy M. Hutson. Reactions of ultracold alkali-metal dimers. *Phys. Rev. A*, 81:060703, 2010.

[85] M. Aymar and O. Dulieu. Calculation of accurate permanent dipole moments of the lowest £+1,3 states of heteronuclear alkali dimers using extended basis sets. *The Journal of Chemical Physics*, 122(20):204302, 2005.

[86] Fudong Wang, Xiaodong He, Xiaoke Li, Bing Zhu, Jun Chen, and Dajun Wang. Formation of ultracold NaRb feshbach molecules. *New Journal of Physics*, 17(3):035003, 2015.

[87] C Becker, P Soltan-Panahi, J Kronjger, S Drscher, K Bongs, and K Sengstock. Ultracold quantum gases in triangular optical lattices. *New Journal of Physics*, 12(6):065025, 2010.

[88] Mikhail Lemeshko, Roman V. Krems, and Hendrik Weimer. Nonadiabatic preparation of spin crystals with ultracold polar molecules. *Phys. Rev. Lett.*, 109:035301, 2012.

[89] André Eckardt. Colloquium: Atomic quantum gases in periodically driven optical lattices. *Rev. Mod. Phys.*, 89:011004, 2017.

[90] Edwin M. Stoudenmire and Steven R. White. Intelligent tensor library. *http://itensor.org/*.

[91] Yi Zhou, Kazushi Kanoda, and Tai-Kai Ng. Quantum spin liquid states. *Rev. Mod. Phys.*, 89:025003, 2017.

[92] Marcel den Nijs and Koos Rommelse. Preroughening transitions in crystal surfaces and valence-bond phases in quantum spin chains. *Phys. Rev. B*, 40:4709–4734, 1989.

[93] Hal Tasaki. Quantum liquid in antiferromagnetic chains: A stochastic geometric approach to the haldane gap. *Phys. Rev. Lett.*, 66:798–801, 1991.

[94] Hiroshi Watanabe, Kiyohide Nomura, and Satoshi Takada. S=1/2 quantum heisenberg ladder and s=1 haldane phase. *Journal of the Physical Society of Japan*, 62(8):2845–2860, 1993.

[95] Yoshihiro Nishiyama, Naomichi Hatano, and Masuo Suzuki. Phase transition and hidden orders of the heisenberg ladder model in the ground state. *Journal of the Physical Society of Japan*, 64(6):1967–1979, 1995.

[96] Steven R. White. Equivalence of the antiferromagnetic heisenberg ladder to a single s=1 chain. *Phys. Rev. B*, 53:52–55, 1996.

[97] Eugene H. Kim, G. Fáth, J. Sólyom, and D. J. Scalapino. Phase transitions between topologically distinct gapped phases in isotropic spin ladders. *Phys. Rev. B*, 62:14965–14974, 2000.

[98] Junjun Xu, Qiang Gu, and Erich J. Mueller. Realizing the haldane phase with bosons in optical lattices. *Phys. Rev. Lett.*, 120:085301, 2018.

[99] Davide Rossini and Rosario Fazio. Phase diagram of the extended bose-hubbard model. *New Journal of Physics*, 14(6):065012, 2012.

[100] Bradraj Pandey, S. Sinha, and Swapan K. Pati. Quantum phases of hard-core bosons in two coupled chains: A density matrix renormalization group study. *Phys. Rev. B*, 91:214432, 2015.